INFORMATION TO USERS

This material was produced from a microfilm copy of the original document. While the most advanced technological means to photograph and reproduce this document have been used, the quality is heavily dependent upon the quality of the original submitted.

The following explanation of techniques is provided to help you understand markings or patterns which may appear on this reproduction.

1. The sign or "target" for pages apparently lacking from the document photographed is "Missing Page(s)". If it was possible to obtain the missing page(s) or section, they are spliced into the film along with adjacent pages. This may have necessitated cutting thru an image and duplicating adjacent pages to insure you complete continuity.

2. When an image on the film is obliterated with a large round black mark, it is an indication that the photographer suspected that the copy may have moved during exposure and thus cause a blurred image. You will find a good image of the page in the adjacent frame.

3. When a map, drawing or chart, etc., was part of the material being photographed the photographer followed a definite method in "sectioning" the material. It is customary to begin photoing at the upper left hand corner of a large sheet and to continue photoing from left to right in equal sections with a small overlap. If necessary, sectioning is continued again — beginning below the first row and continuing on until complete.

4. The majority of users indicate that the textual content is of greatest value, however, a somewhat higher quality reproduction could be made from "photographs" if essential to the understanding of the dissertation. Silver prints of "photographs" may be ordered at additional charge by writing the Order Department, giving the catalog number, title, author and specific pages you wish reproduced.

5. PLEASE NOTE: Some pages may have indistinct print. Filmed as received.

Xerox University Microfilms
300 North Zeeb Road
Ann Arbor, Michigan 48106

75-20,379

KARRENBROCK, Anthony Henry, 1946-
STRUCTURE DETERMINATION OF [(CH3)3Si]3SiH, INFRARED INVESTIGATION OF IF7, AND AN APPLICATION OF THREE-ATOM SCATTERING THEORY TO IF7 AND ReF7.

The University of Michigan, Ph.D., 1975
Chemistry, physical

Xerox University Microfilms, Ann Arbor, Michigan 48106

THIS DISSERTATION HAS BEEN MICROFILMED EXACTLY AS RECEIVED.

STRUCTURE DETERMINATION OF $[(CH_3)_3Si]_3SiH$, INFRARED INVESTIGATION OF IF_7, AND AN APPLICATION OF THREE-ATOM SCATTERING THEORY TO IF_7 AND ReF_7

by

Anthony Henry Karrenbrock

A dissertation submitted in partial fulfillment
of the requirements for the degree of
Doctor of Philosophy
(Chemistry)
in The University of Michigan
1975

Doctoral Committee:

Professor Lawrence S. Bartell, Chairman
Professor Samuel Krimm
Professor Robert L. Kuczkowski
Associate Professor Ralph W. Rudolph

ACKNOWLEDGEMENTS

I wish to thank Professor Lawrence S. Bartell for his support, his helpful discussions, and his patience during the research and the writing of this dissertation.

I also wish to thank the members, past and present, of the electron diffraction group, and in particular, Mr. David Romenesko, for their generous and valuable help. Special thanks go to Dr. William F. Bradford for all his help and long-standing friendship, to Mrs. Monique Seibel for her superb figures, to Mrs. L. Myers for her patience in typing this dissertation, and to Messrs. N. Johnston, W. Wolf, and E. Metzger of the Instrument Shop for some of the equipment.

Finally I extend my appreciation to all my friends from Ann Arbor and St. Louis for their encouragement and support throughout the course of this work.

The financial support of the National Science Foundation, The University of Michigan Computing Center, and the Department of Chemistry is gratefully acknowledged.

TABLE OF CONTENTS

ACKNOWLEDGEMENTS ii

LIST OF TABLES v

LIST OF FIGURES vi

LIST OF APPENDICES vii

PART I. ELECTRON DIFFRACTION INVESTIGATION OF $[(CH_3)_3Si]_3SiH$ 1

INTRODUCTION 2

EXPERIMENTAL 3

ANALYSIS OF DATA 4

MOLECULAR MODEL 10

RESULTS 17

DISCUSSION 34

SUMMARY 40

REFERENCES 41

PART II. LOW TEMPERATURE INFRARED INVESTIGATION OF IF_7 42

ELECTRON DIFFRACTION AND STRUCTURAL INVESTIGATION OF IF_7 43

PSEUDOROTATION IN IF_7 46

SPECTROSCOPIC INVESTIGATIONS OF IODINE HEPTAFLUORIDE 49

MATRIX ISOLATION INVESTIGATION OF IODINE HEPTAFLUORIDE 54

EXPERIMENTAL 59

ANALYSIS OF DATA 66

RESULTS 68

IF_7 IN AN ARGON MATRIX 68

SOLID IF_7 AT LIQUID NITROGEN TEMPERATURE 71

IF_7 IN A XENON MATRIX 71

IF_7 IN A NITROGEN MATRIX 76

SOLID IF_7 AT LIQUID HELIUM TEMPERATURE 76

DISCUSSION 82

CONCLUSION 86

REFERENCES 87

PART III. THREE-ATOM SCATTERING IN ReF_7 AND IF_7 . . . 89

THREE-ATOM SCATTERING 91

PARAMETER ALTERATIONS 101

CONCLUSION 106

REFERENCES 108

APPENDICES 109

LIST OF TABLES

1.1	Experimental Conditions for $[(CH_3)_3Si]_3SiH$ . .	5
1.2	Molecular Description for $[(CH_3)_3Si]_3SiH$ . . .	14
1.3	Structural Parameters and Estimated Uncertainties for $[(CH_3)_3Si]_3SiH$ (Blended Camera Distances)	26
1.4	Structural Parameters and Estimated Uncertainties for $[(CH_3)_3Si]_3SiH$ (Middle Camera Distance)	27
1.5	Correlation Matrix for Blended Camera Distances	28
1.6	Correlation Matrix for Middle Camera Distance .	30
1.7	Correlation Matrix Elements	32
1.8	Structural Parameters and Estimated Uncertainties for $[(CH_3)_3Si]_3SiH$ and $[(CH_3)_3Si]_4Si$	36
2.1	Fundamental Vibrations of IF_7, IOF_5, IF_5 (Gas Phase)	50
2.2	Vibrational Assignments for IF_7	51
2.3	Combinations of $e_2"$ with D_{5h} Symmetry Species .	57
2.4	IF_7/Ar, Liquid Helium Temperature	70
2.5	Solid IF_7, Liquid Nitrogen Temperature	70
2.6	IF_7/Xe, Liquid Helium Temperature	75
2.7	IF_7/N_2, Liquid Helium Temperature	78
2.8	Solid IF_7, Liquid Helium Temperature	81
3.1	IF_7 Three-Atom Input, C_2 Conformation	94
3.2	IF_7, C_2 Conformation: Parameters and Estimated Uncertainties	103
3.3	ReF_7, C_2 Conformation: Parameters and Estimated Uncertainties	104

LIST OF FIGURES

1.1	Representation of $[(CH_3)_3Si]_3SiH$	12
1.2	Silicon Tilt Geometric Arrangement	16
1.3	Experimental and Calculated Reduced Molecular Intensities	18
1.4	Fourier Sine Transform of the Calculated and Experimental Reduced Molecular Intensities with the Difference Curve (Blended Camera Distances)	20
1.5	Fourier Sine Transform of the Calculated and Experimental Reduced Molecular Intensities with the Difference Curve	23
2.1	D_{5h} Bending Coordinates	45
2.2	Conformations for IF_7	47
2.3	Cryostat and IR Cell	62
2.4	IR Cell	63
2.5	IF_7/Ar, Liquid Helium Temperature	69
2.6	Solid IF_7/Liquid N_2	72
2.7	IF_7/Xe, Liquid Helium Temperature	74
2.8	IF_7/N_2, Liquid Helium Temperature	77
2.9	Solid IF_7, Liquid Helium Temperature	79
3.1	Three-Atom Corrections and Residuals from Least Squares of the Intensities Refinement (IF_7)	98
3.2	Three-Atom Corrections and Residuals from Least Squares of the Intensities Refinement (ReF_7)	101

LIST OF APPENDICES

A. Experimental Leveled Intensity and Background Intensity Functions for $[(CH_3)_3Si]_3SiH$ 109

B. Conformational Analysis 112

C. Electron Diffraction Study of $[(CH_3)_3Si]_3CH$ . . . 119

D. Computer Programs 123

PART I. ELECTRON DIFFRACTION INVESTIGATION OF $[(CH_3)_3Si]_3SiH$.

INTRODUCTION

A gas phase electron diffraction investigation of tris(trimethylsilyl)silane was undertaken to determine the molecule's structure. The study was also undertaken to elucidate the effects of bulky functional groups in proximity to one another. Previous structural determinations including tetrakis(trimethylsilyl)silane are available for comparison with the present work. The hydrocarbon analog of tris(trimethylsilyl)silane is tri-tert-butylmethane, which Bartell and Bürgi investigated by gas phase diffraction. They reported severe steric strain due to the close packing of three t-butyl groups around a single carbon atom. The results of the present work are compared with TTBM to reveal the effects of the Si-C and the Si-Si bond lengths on steric strain as opposed to the C-C lengths in TTBM.

Tris(trimethylsilyl)silane was subjected to a molecular mechanics study in an attempt to extend the work of Jacob, Thompson, and Bartell to silanes. The results of a conformational analysis with a modified force field based partly on Allinger's previous work[1] are presented in Appendix B.

Gas phase diffraction patterns of tris(trimethylsilyl)methane were taken. However, the analysis was not completed because the compound decomposed during or prior to the experiment. Details of this study are presented in Appendix C.

EXPERIMENTAL

Approximately three grams of tris(trimethylsilyl)-silane were received from Dr. Hans Bürger*.[2] The sample arrived in a glass tube with a ground tapered joint and a vacuum break seal and was transferred without further purification to a Monel tank equipped with a high vacuum Hoke valve. Vapor pressure measurements indicated that the compound would have to be heated to 130°C to achieve sufficient pressure for diffraction camera exposures of several seconds.

A platinum tip with a throat diameter of 0.3 mm was attached to a jacketed nozzle, and the entire assembly was mounted through an adjustable bellows into the diffraction camera. The Monel sample tank and the nozzle were joined by a jacketed Monel tube which could be isolated from the nozzle by a Monel valve. The sample introduction line valve was wrapped with several turns of copper tubing soldered to the valve's external surface. A heater-circulator with an auxiliary pump forced ethylene glycol through the jackets and tubing to heat the sample introduction system. The Monel tank was immersed in a Dewar filled with ethylene glycol, heated by the same heater-circulator. The temperature of the heating system was controlled by a thermoregulator and monitored with several

---

* Institut für Anorganische Chemie der Technischen Universität, 33 Braunschweig, Germany.

thermometers, reading to tenths of a degree. The entire heating assembly and sample line were insulated.

Before heating and pressurizing the introduction line, the sample tank was cooled with liquid nitrogen and then opened to the vacuum pumps to remove trapped air. Gas phase diffraction patterns were recorded on 4 x 5 inch Kodak Electron Image (Selected Flat) plates with the University of Michigan diffraction camera[3] operated at 40 kV. Plates were exposed at the 21 cm (long) and the 11 cm (middle) camera distances with the radius-cubed (r^3) rotating sector and at the 21 cm camera distance with the radius-squared (r^2) sector. Development of the plates was in Kodak HRP developer agitated with a nitrogen gas-burst system for 3 minutes at 20°C. To retard fogging of the plates, 1 gram of benzotriazole was added to each liter of the developing solution. All plates were dried in a vacuum chamber for at least 24 hours to remove adsorbed water before loading the plate box into the camera. Experimental conditions are listed in Table 1.1.

ANALYSIS OF DATA

Electron diffraction intensities are measured by a digital recording, single beam microphotometer. Photodetector voltages, which are the output of a photocell and which are proportional to the light transmitted through the plate, are recorded at 0.125 mm intervals across the

Table 1.1

Experimental Conditions for $[(CH_3)_3Si]_3SiH$

	I	II	III
Camera distance (cm)	21.674	10.648	21.235
Sector (radius, mm)	r^3 (48)	r^3 (48)	r^2 (32)
Nozzle temperature (°C)	127	130	120
Sample pressure (torr)	30	30	27
Exposure time (sec)	1	8	0.6
Beam current (μA)	0.70	0.56	0.70
Nozzle tip diameter (mm)	0.3	0.3	0.3
Number of plates	4	4	4
Nozzle to beam distance (mm)	0.050	0.050	0.050

diameter of the plate. The plates are spun at 180 rpm to measure an area exposed to at least 10^7 electrons for improved counting statistics.

A total of 705 readings are made for r^3 sector plates, but 103 voltages across the center are discarded (because the center of the plate is blocked by the beam trap in the center of the sector), leaving 602 voltage readings. Averaging the voltages of corresponding radii across the center results in 301 voltages of which every other value is subjected to the structural analysis. For the r^2 sector plates, 401 voltages are initially measured. Across the center of the plate, 67 readings are discarded, and the remaining 334 values are averaged, leaving 167 voltage measurements for analysis.

The averaged voltages from the recording microphotometer are transformed into absorbances (or optical densities) from which the intensities in terms of exposure may be derived[4] according to the following equation:

$$E = A + 0.100\ A^2 + 0.1333\ A^3 + 0.002\ A^4 \qquad (1)$$

where A is absorbance and E is exposure. The intensities are corrected for imperfections in the rotating sector and for exposure on a flat rather than a spherical plate. Each intensity point is associated with a plate radius and corresponds to a particular value of the scattering angle variable, s, where $s = (4\pi/\lambda)\sin(\phi/2)$. The scattering

angle is ϕ, and λ is the De Broglie wavelength of the 40 kV electron beam ($\lambda \sim 0.06$ A°).

The data of several photographic plates (see Table 1.1) for a given camera distance were averaged. The s values were converted to q where $q = (10/\pi)s$. The averaged intensities were interpolated to integral q values by a four-point Lagrangian method. The averaging and interpolation produced 32 intensity points for the 21 cm (r^2 sector) camera distance, 57 points for the 21 cm (r^3 sector) camera distance, and 100 points for the 11 cm (r^3 sector) camera distance.

Background functions, $I_B(q)$, were calculated with the following equation:

$$I_B(q) = A \exp(-\alpha q) + \sum_{n=o} a_n q^n \qquad (2)$$

Background functions were calculated separately for the data of each camera distance. Linear five term polynomial functions were calculated for the 21 cm (r^2 sector) data and for the 11 cm (r^3 sector) data. The 21 cm (r^3 sector) intensities had a five term polynomial plus an exponential term with $\alpha = 0.2772$. The experimental intensities, taken as the sum of molecular and atomic components,

$$I_{total} = I_{mol} + I_{at} \qquad (3)$$

were leveled in the usual manner to give,

$$\frac{I_{total}}{I_{at}} = \frac{I_{mol}}{I_{at}} + 1 \qquad (4)$$

where $I_{total}/I_{at} = I_o$, the leveled intensity and $I_{mol}/I_{at} = M(q)$, the reduced molecular intensity.[3] The atomic intensities and the reduced molecular intensities were computed with the partial wave elastic scattering factors of Schafer, Yates, and Bonham.[5] The inelastic scattering factors were obtained from Tavard, Nicolas, and Rouault.[6] Tables of s, $I_o(s)$, and $I_B(s)$ for each camera distance are presented in Appendix A.

The reduced molecular intensities of the individual camera distances were refined separately by a least squares procedure.[7] After this preliminary refinement, the data of all three camera distances were blended into the composite reduced molecular intensities which are subjected to the least squares refinement. No more than two sets of intensity points at equal q values from separate camera distances may be blended. Consequently in the overlap regions certain intensity points were not included in the composite intensity. The excluded intensities are reported without background points in Appendix A. The current geometrically constrained least squares program for analysis of the intensities designated as LSI, was redimensioned to accommodate 200 internuclear distances instead of 150. The new program, called AHKLSI, required a new subroutine package which was redimensioned to 200 distances. The

standard READQ subroutine was designated as AHKRED and the remaining subroutines called AHKSUB.

Morse asymmetry constants[8,9] for all interatomic distances were chosen to be 2.0 $A^{\circ -1}$, and no shrinkages were taken into account for the molecule. For the initial refinement, the contribution of the H···H scattering was calculated and, except for the H···H(1,3) distance, was subtracted from the leveled intensities. There are 97 H···H distances which contribute only a small portion to the total scattering since nuclear pair scattering is proportional to the product of the respective atomic numbers. As the refinement progressed, the H···H scattering was added back to the leveled intensities for completion of the structural determination.

In the least squares analysis, weighting of the intensities was proportional to $q^2 \times P(q)$ where P(q) represents a plateau function. In treating the camera distances separately, the 21 cm (r^2 sector) data at small q were found to be less reliable than the larger q data. So a plateau function was devised to give the intensities at larger q greater weight than the intensities at small q. The plateau function is of the form:

$$P(q) = \{A - \exp[-a(q - q_a)^2]\} \qquad (5)$$

where A = 1.25, a = 1.02537×10^{-3}, and q_a = 4.0. The total weighting function rises sharply as q increases but

then levels off around $q = 40$ A°$^{-1}$. Weighting proportional to q^2 alone could not produce the necessary abrupt rise in the weights.

MOLECULAR MODEL

Tris(trimethylsilyl)silane contains 41 atoms ($C_9Si_4H_{28}$) and is represented in Figure 1.1 which is not drawn to scale. Accordingly, there are potentially 820 internuclear distances based on the formula, $n(n - 1)/2$ where n is the number of atoms in the molecule.[3] Not all of the 820 distances are distinct. Several assumptions concerning the symmetry of the molecule were made in order to reduce the number of independent internuclear distances and to simplify the structural problem.

All the hydrogen atoms are bonded to methyl carbons except for the one hydrogen which is bonded to the tertiary silicon atom. The first assumption is that all C-H bond lengths are equal. The next assumption is that the methyl groups undergo little torsional strain and that all the $Si\text{-}C\text{-}H_{methyl}$ angles are equal. Previous structural studies of silanes[10,11] indicated C-Si bond lengths of 1.8 A° and Si-Si bond lengths of 2.3 A° which are significantly longer than typical C-C bond lengths, e.g., 1.54 A°.

All methyl groups are constrained to a staggered configuration with respect to the quaternary silicon atom and the other methyl groups of the same trimethylsilyl sub-

Figure 1.1. Representation of $[(CH_3)_3Si]_3SiH$

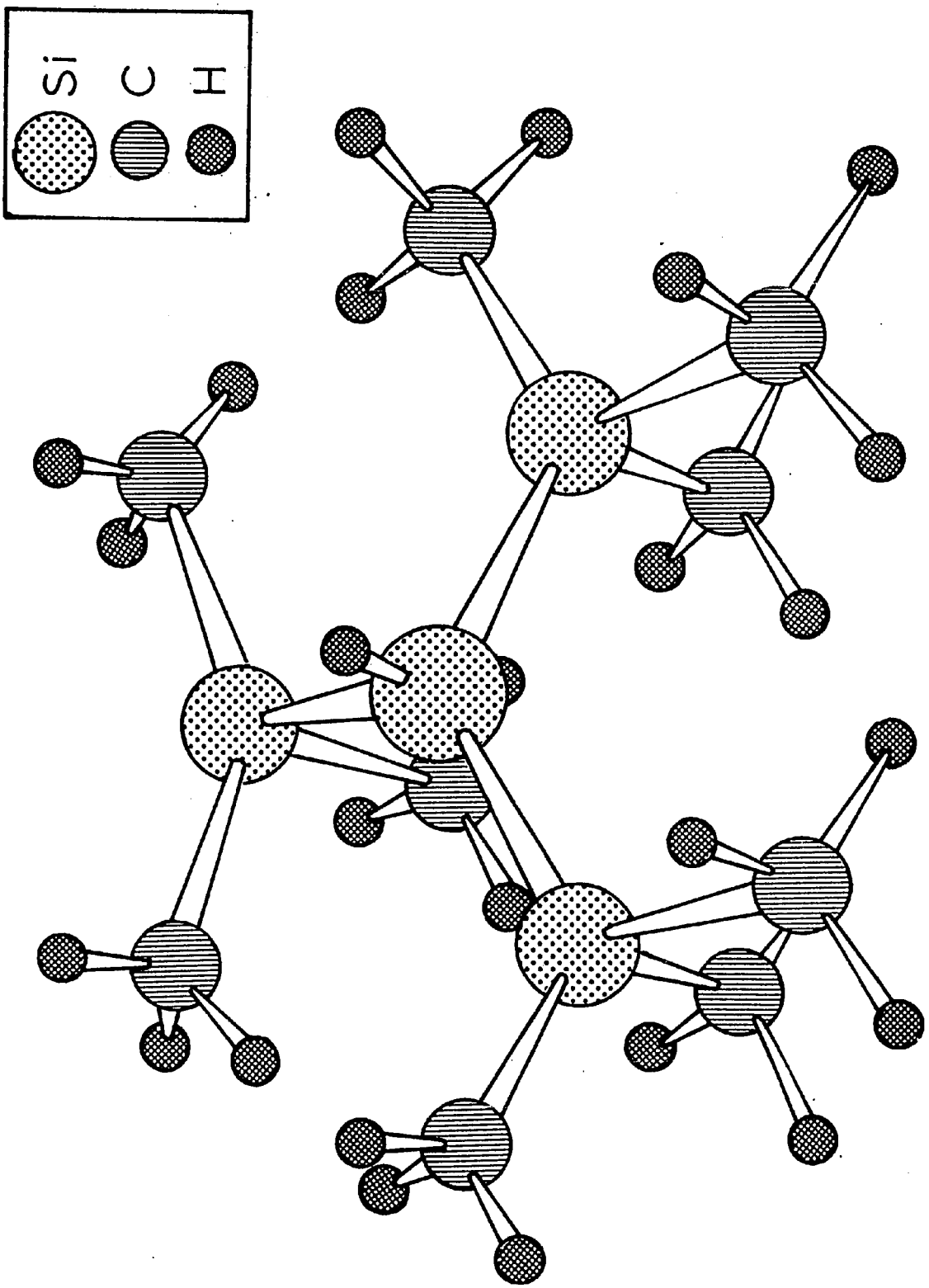


Figure 1.1.

group. In terms of symmetry, the constraint imposed on the methyl groups results in C_{3v} local symmetry on each of the three trimethylsilyl groups. In order to maintain the local C_{3v} symmetry, all C-Si-Si angles were taken to be equal.

The final assumption involves the torsional angles of the trimethylsilyl groups. The various angle combinations which were tested will be discussed in a later section. The assumption is that the three trimethylsilyl groups have the same torsional angle with respect to the axis through the Si-H bond. This constraint gives the molecule overall C_3 symmetry with the C_3 rotational axis coincident with the Si-H bond.

For simplicity in the molecular description, 12 "dummy" atoms which have no mass or nuclear charge are included. The dummy atoms are assigned appropriate coordinates and exist strictly for bookkeeping purposes only. A dummy atom is superimposed on each of the trimethylsilyl silicon atoms and one on each of the carbons. The advantage of the dummy atoms is to permit the rotation of the entire trimethylsilyl group by altering only the torsional angle of the dummy atom. The methyl dummy atoms in turn can rotate the methyl groups. Without such dummy atoms, the molecular description for the least squares analysis would be much more complicated for an already formidable problem. A complete list of the structural parameters is given in Table 1.2.

Table 1.2

Molecular Description for $[(CH_3)_3Si]_3SiH$

Geometric Parameters

Number	Parameter	Torsion
1	Si-H(1)	Bond
2	Si-Si	Bond
3	Si-C	Bond
4	C-H	Bond
5	C-Si-H(1)	Angle
6	C-Si-Si	Angle
7	Si-C-H(methyl)	Angle
8	C-Si-Si-H(1)	Torsion
9	Si-Si-C-H(methyl)	Torsion
10	Silicon Tilt	Angle

Amplitudes of Vibration

Number	Parameter	
1	Si-Si	(1,2)
2	Si-C	(1,2)
3	Si-H	(1,2)
4	C···C	(1,3)
5	C-H	(1,2)
6	H···H	(1,3)
7	Si···Si	(1,3)
8	Si···C	(1,3)
9	Si···C	(1,4)G[a]
10	Si···C	(1,4)T[b]
11	Si···H[c]	(1,3)
12		
13	C···C	(1,5)TG
14	C···C	(1,5)TT
15	C···C	(1,5)GG
16	C···H	(1,4)
17	C···H	(1,6)
18	H···H	Long 1
19	H···H	Long 2
20	H···H	Long 3

[a] gauche.

[b] trans.

[c] All Si···H amplitudes other than the (1,3) amplitude.

The incorporation of the dummy atoms is beneficial in another respect. A novel aspect of this molecular description is the inclusion of "bent bonds" at the tertiary silicon atoms. The concept of a bent bond is not entirely new and has been previously discussed.[11] The bent bond parameter is designated as the Silicon Tilt angle with a value of 0.0° when no bending is present. Figure 1.2 depicts the geometric arrangement. Note that the dummy atom and the tertiary silicon atom are superimposed because they are joined by a bond length of 0.0 A°. Nevertheless, the methyl groups can be displaced by altering the tilt angle while the value of the Si-Si-H(1) angle remains constant. On a practical level, this is accomplished by varying the Si-Dummy-Si, or tilt, angle. Obviously it is much easier to alter the tilt angle than to change independently the various angles formed by the methyl carbons and the Si-Si bonds.

Initial values for the molecular model parameters are from published structures and in particular the values from tetrakis(trimethylsilyl)silane.[11] To test the model and the initial parameter values, a molecular mechanics study was undertaken. The results of the conformational analysis are presented and discussed in Appendix B.

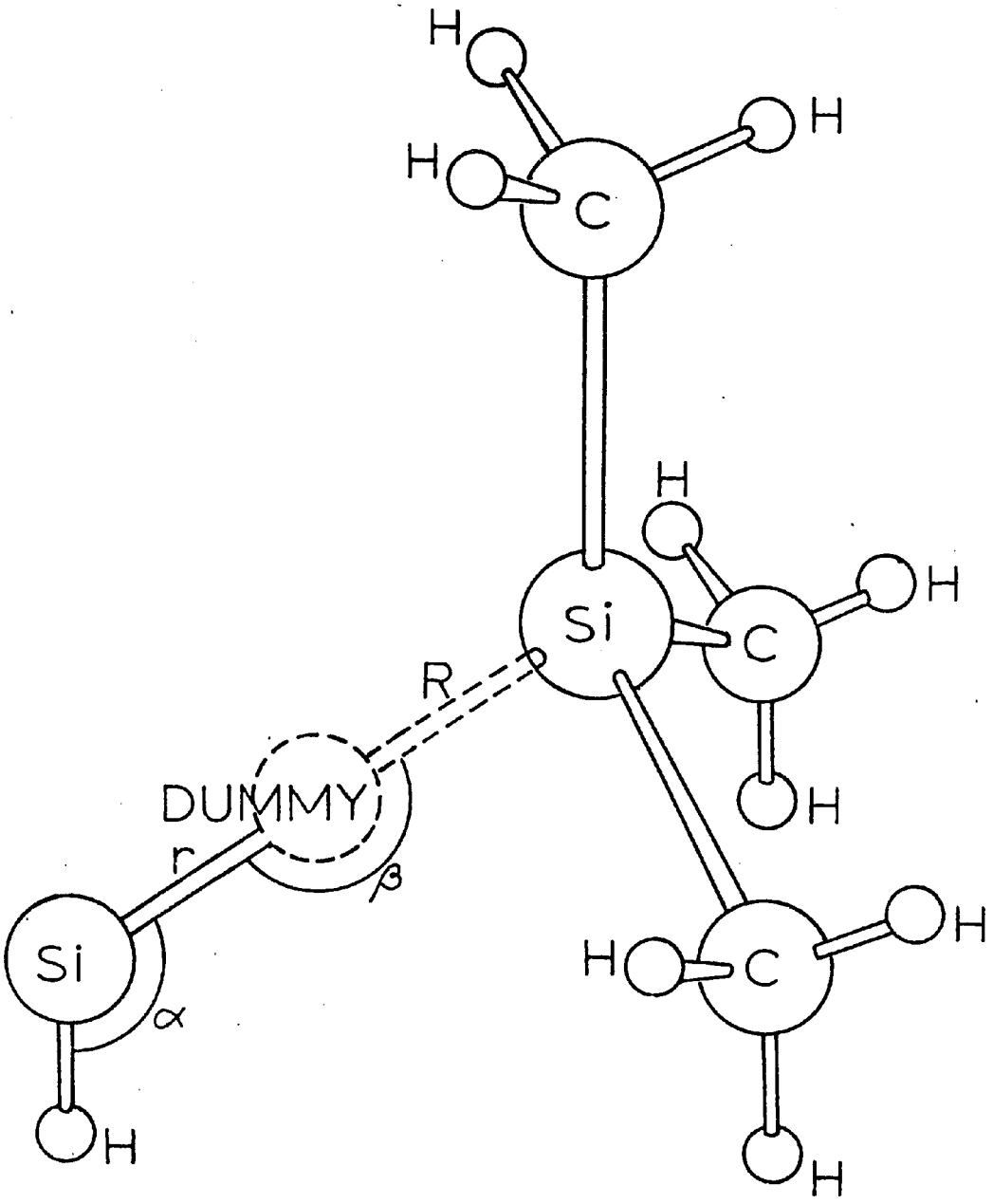


Figure 1.2. Silicon Tilt Geometric Arrangement.

RESULTS

Tables of the scattering variable, s, leveled intensities, I_o, and the background, I_B, are presented in Appendix A. The experimental and calculated molecular intensities, sM(s), for the blend of three camera distances are compared in Figure 1.3. A difference curve between the experimental and calculated curves is included with the intensities.

Radial distribution functions with integral termination correction and the Degard damping factor, $\exp(-bs^2)$, where $b = 0.0015$ A°^{2}, were calculated. Two radial distribution functions were calculated for comparison with the Fourier transform of the experimental M(s) values. In Figure 1.4, the Fourier sine transform of the composite M(s) intensities blended from the two long camera distances and the middle distance data is depicted. Below the experimental curve is the difference curve between the calculated and the experimental values. The difference curve shows significant deviations of the experimental data from the theoretical model between 1 A° and 3 A°. The leading edge of the Si-C peak at 1.88 A° exhibits an unexpected shoulder corresponding to a peak centered near 1.6 A°.

An examination of the individual camera distance data revealed that the transform of the 21 cm (r^3 sector) data contained the 1.6 A° peak, displaying the shoulder which

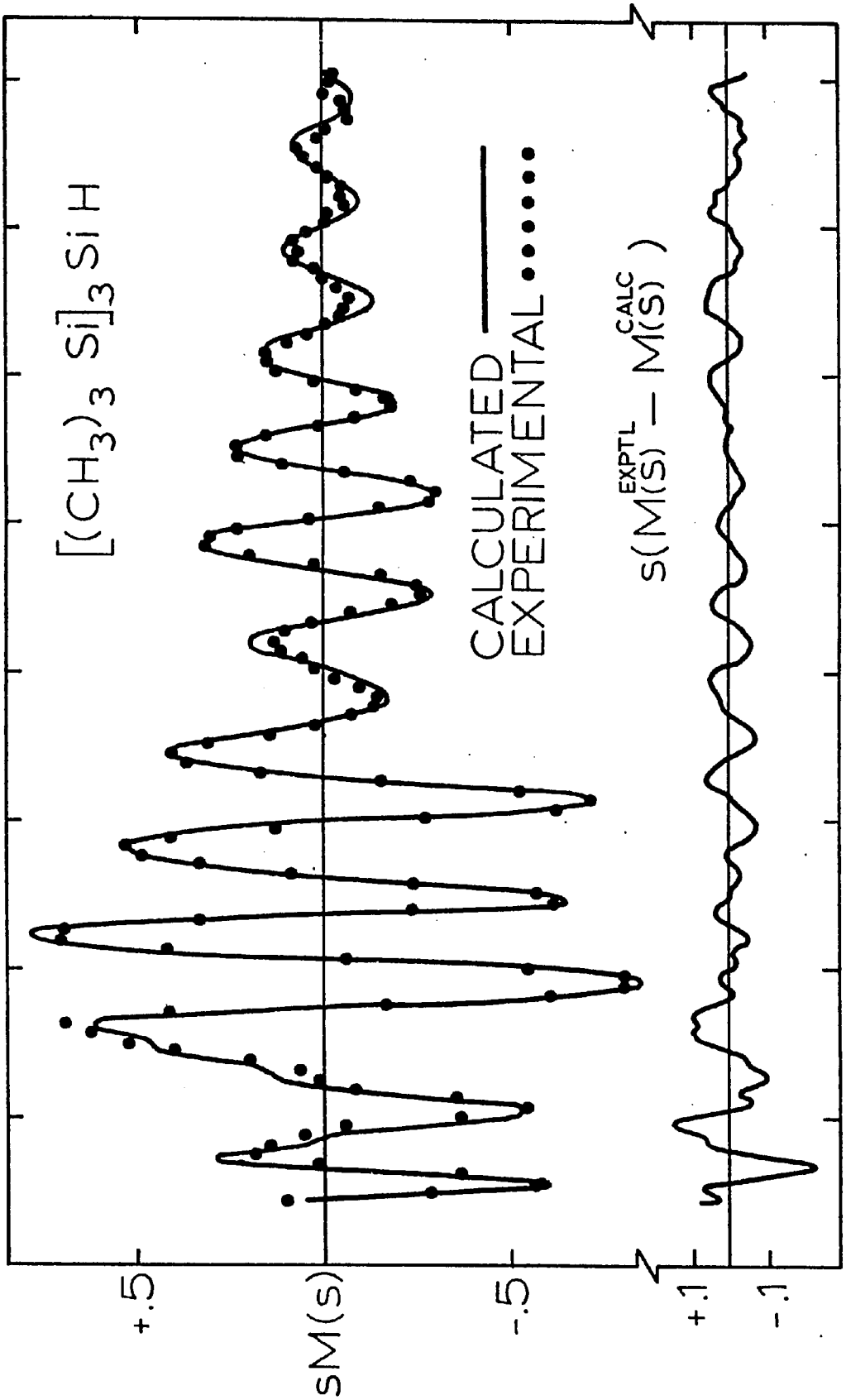


Figure 1.3. Experimental and Calculated Reduced Molecular Intensities.

Figure 1.4. Fourier Sine Transform of the Calculated and Experimental Reduced Molecular Intensities with the Difference Curve.

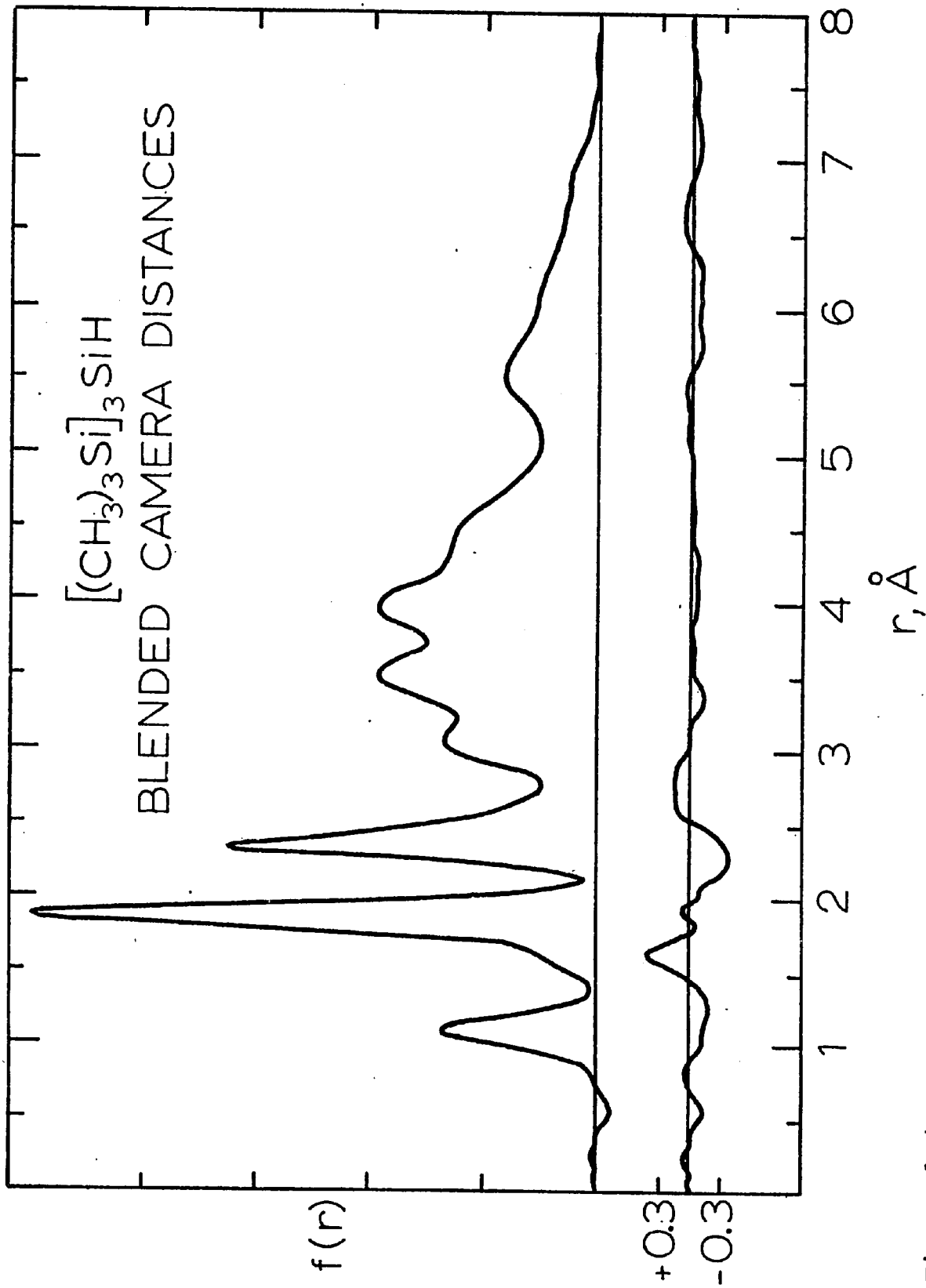


Figure 1.4.

appears in Figure 1.4 on the Si-C peak at 1.882 A°. On the other hand, the 21 cm (r^2 sector) and 11 cm (r^3 sector) intensities did not contain the 1.6 A° peak to the extent of the 21 cm (r^3 sector) data. Experimentally, the 21 cm (r^3 sector) intensities were obtained first. Thus the extraneous peaks in the intensities appear to be due to a solvent or some by-product of the synthesis. The impurity could then have been removed from the sample during the early experimental stages. When the 21 cm (r^2 sector) data and the 11 cm data were recorded, presumably the concentration of the impurity had decreased as the silane sample was depleted.

The 11 cm camera distance intensities were analyzed alone by the least squares method and the resulting f(r) is presented in Figure 1.5. The discrepancies between the experimental and theoretical curves in the region from 1 A° to 3 A° are much smaller for the 11 cm data alone than for the blended data. A trace of the 1.6 A° peak remains but is significantly less than in the curve for the blended data. It must be emphasized that the blended data begins at s = 2.091 $A°^{-1}$ whereas the 11 cm data begins at s = 8.806 $A°^{-1}$. In deriving an f(r) curve, the region between s = 0 $A°^{-1}$ and the first experimental s value is represented by theoretical points. The 11 cm data therefore has an f(r) with more theoretical points in the low s region than the blended data. Thus some of the improvement may be attributed to the increased theoretical

Figure 1.5. Fourier Sine Transform of the Calculated and Experimental Reduced Molecular Intensities with the Difference Curve.

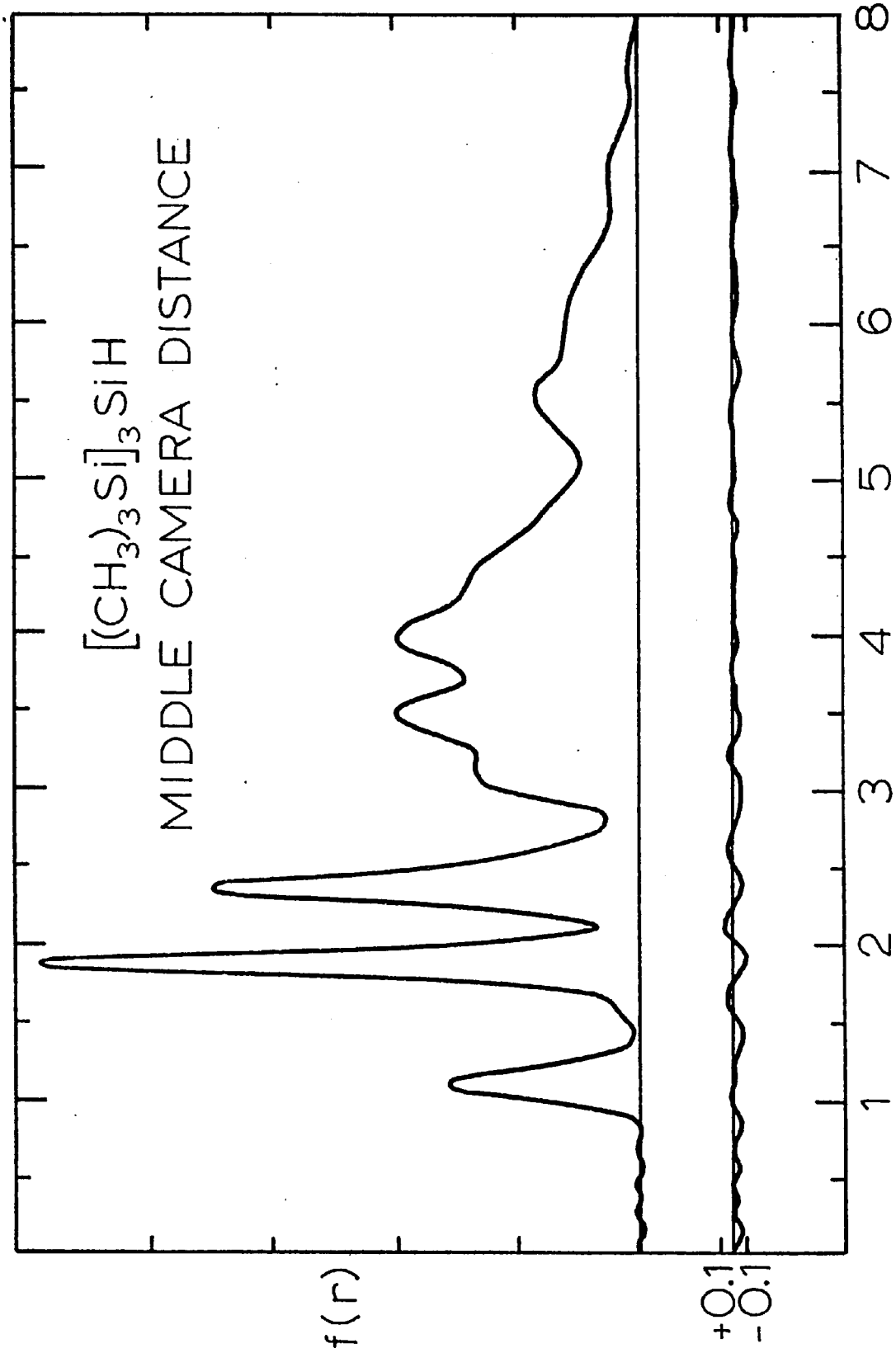


Figure 1.5.

contribution to the curve.

Error estimates on the peak position of the Si-C bond and the Si-Si bond and the corresponding amplitudes of vibration in the blended f(r) were calculated with formulas published by Bonham and Bartell.[7] The f(r) peak at 1.882 A° for the Si-C bond length has an amplitude of vibration, l_{ij}, equal to 0.0575 A°. The estimated errors are $\sigma[r(Si-C)] = \pm 0.010$ A° and $\sigma[\ell(Si-C)] = \pm 0.010$ A°. The estimated errors for both the Si-Si bond length and the Si-Si amplitude were the same at ± 0.010 A°.

The C-H, Si-C, and Si-Si bonded distance peaks are quite apparent in the f(r) curves. The various (1,3) nonbonded distances occur above 3 A° but below 4.5 A°. There is a great deal of overlap in this region above 3.5 A°. Nevertheless the difference curve is small, indicating good agreement between the theoretical model and the experimental intensities.

The intensities of the 11 cm data alone cannot provide sufficient information for an accurate conformation determination. Furthermore the 21 cm (r^2 sector) data was not of the highest quality for blending with the 11 cm intensities. The r^2 sector data had a rather low index of resolution ($R = \frac{M^{exp}_{(s)}}{M^{th}_{(s)}}$) relative to the 11 cm intensities (see Table 1.3). So despite the obvious deficiencies of the 21 cm (r^3 sector) data, these intensities were blended with the other two intensity sets.

The 21 cm (r^2 sector) data were blended with the other intensity sets but weighted down with a plateau function. The actual weight function was $P(q) \times q^2$ as described earlier. The blended intensities or composite molecular intensities were analyzed, and the results are presented in Table 1.3. Varying only the bonded parameters and appropriate amplitudes, the 11 cm data were analyzed, but the angles and torsions of the molecule were held constant. The results of the 11 cm data analysis are reported in Table 1.4. The estimated uncertainties which appear in Tables 1.3 and 1.4 take into account both random and systematic errors. The systematic errors are estimated as follows: 4 parts per ten thousand (pptt) in the camera distance measurement, 2 pptt in the electron beam wavelength, and 2 pptt in the photographic plate radii as measured by the microphotometer. Error estimates for distances less than 2.6 A° and their corresponding amplitudes have been corrected to the bona fide error matrix, M_x^w, error estimates.[14]

A matrix of correlation coefficients for the blended data and another for the 11 cm intensities are presented in Tables 1.5 and 1.6, respectively. Parameters and their notation for the correlation matrices are listed in Table 1.7. The matrices result from the least squares analysis of the composite molecular intensity for the blended camera distances and for the separate analysis of the 11 cm camera distance intensities. A diagonal weight matrix

Table 1.3

Structural Parameters[a] and Estimated Uncertainties[b] for $[(CH_3)_3Si]_3SiH$ (Blended Camera Distances)

Parameter	r_g	l_g	Angle
Si-H(1)	1.484[c]	0.127[c]	
Si-Si	2.357 ± 0.008	0.070 ± 0.015	
Si-C	1.882 ± 0.004	0.058 ± 0.007	
C-H	1.114 ± 0.013	0.082 ± 0.020	
Si-Si-H(1)			103.9 ± 2.0
C-Si-Si			110.5 ± 0.8
Si-C-H			109.8 ± 2.1
C-Si-Si-H(1)			57.4 ± 4.4
H-C-Si-Si[c]			0.0
Silicon Tilt[c]			0.0
C···C(1,3)	3.052 ± 0.018	0.105 ± 0.018	
Si···Si(1,3)	3.962 ± 0.030	0.133 ± 0.022	
Si···C(1,3)	3.493 ± 0.018	0.148 ± 0.020	

R = 0.93 ± 0.06 Middle Distance (r^3 sector)
R = 0.86 ± 0.06 Long Distance (r^3 sector)
R = 0.69 ± 0.06 Long Distance (r^2 sector)

$\sigma(I)/\langle I\rangle = 0.0013$

[a] Distances and amplitudes reported in A°, angles in degrees.

[b] Estimated uncertainties include the effects of both random and systematic errors[14] and are reported as 2σ except for $\sigma(I)/\langle I\rangle$.

[c] Not-varied, see text.

Table 1.4

Structural Parameters[a] and Estimated Uncertainties[b] for $[(CH_3)_3Si]_3SiH$ (Middle Camera Distance)

Parameter	r_g	l_g	Angle
Si-H(1)	1.484[c]	0.127[c]	
Si-Si	2.353 ± 0.006	0.067 ± 0.010	
Si-C	1.885 ± 0.002	0.055 ± 0.005	
C-H	1.114 ± 0.010	0.074 ± 0.010	
Si-Si-H(1)			103.9 ± 2.2
C-Si-Si			110.5 ± 1.6
Si-C-H			109.8 ± 3.0
C-Si-Si-H(1)			57.4 ± 6.0
H-C-Si-Si[c]			0.0
Silicon Tilt[c]			0.0
C···C(1,3)	3.058 ± 0.032	0.105 ± 0.016	
Si···Si(1,3)	3.955 ± 0.036	0.132 ± 0.018	
Si···C(1,3)	3.493 ± 0.034	0.141 ± 0.028	

R = 0.93 ± 0.05

$\sigma(I)/\langle I\rangle$ = 0.0010

[a] Distances and amplitudes reported in A°, angles in degrees.

[b] Estimated uncertainties include the effects of both random and systematic errors[14] and are reported as 2σ except for $\sigma(I)/\langle I\rangle$.

[c] Not varied, see text.

Table 1.5

Correlation Matrix for Blended Camera Distances

	ϕ_1	ϕ_2	ϕ_3	ϕ_4	ϕ_5	ϕ_6	ϕ_7	ϕ_8	ϕ_9	ϕ_{10}
ϕ_1	1.00	0.03	0.00	0.28	-0.16	-0.24	-0.03	0.02	0.06	-0.01
ϕ_2		1.00	-0.03	0.07	0.03	-0.30	-0.05	-0.23	-0.33	0.24
ϕ_3			1.00	0.02	-0.01	-0.17	0.005	0.03	0.04	0.01
ϕ_4				1.00	-0.10	-0.16	-0.08	-0.02	-0.05	0.09
ϕ_5					1.00	0.16	-0.14	0.04	0.08	0.27
ϕ_6						1.00	0.01	-0.07	0.24	-0.27
ϕ_7							1.00	0.03	0.04	-0.03
ϕ_8								1.00	0.40	0.01
ϕ_9									1.00	-0.08
ϕ_{10}										1.00
ϕ_{11}										
ϕ_{12}										
ϕ_{13}										
ϕ_{14}										
ϕ_{15}										
ϕ_{16}										
ϕ_{17}										
ϕ_{18}										
ϕ_{19}										

Table 1.5 continued.

	ϕ_{11}	ϕ_{12}	ϕ_{13}	ϕ_{14}	ϕ_{15}	ϕ_{16}	ϕ_{17}	ϕ_{18}	ϕ_{19}
ϕ_1	0.04	-0.04	-0.003	0.01	0.04	0.04	0.65	-0.10	0.09
ϕ_2	-0.18	-0.76	-0.06	-0.16	-0.01	-0.02	-0.10	0.04	-0.44
ϕ_3	-0.03	0.04	-0.002	0.01	0.03	0.01	0.02	-0.02	0.06
ϕ_4	-0.03	-0.08	0.03	-0.21	-0.12	0.07	0.16	-0.32	-0.06
ϕ_5	0.04	0.05	0.06	-0.26	-0.09	0.002	-0.10	0.60	0.10
ϕ_6	0.14	0.32	0.02	0.16	-0.06	0.01	-0.04	0.12	0.32
ϕ_7	0.02	0.05	-0.09	0.11	0.00	-0.15	-0.01	-0.24	0.05
ϕ_8	0.21	0.34	0.08	0.05	0.04	0.04	0.13	0.004	0.50
ϕ_9	0.33	0.45	0.10	0.13	0.03	0.06	0.31	0.04	0.78
ϕ_{10}	-0.05	-0.27	0.03	-0.25	0.01	0.002	-0.15	0.09	-0.12
ϕ_{11}	1.00	0.25	0.06	0.07	0.02	0.03	0.17	0.02	0.42
ϕ_{12}		1.00	0.08	0.15	0.02	0.04	0.16	0.01	0.61
ϕ_{13}			1.00	-0.26	0.32	-0.01	0.04	0.17	0.13
ϕ_{14}				1.00	-0.16	0.03	0.09	-0.32	0.17
ϕ_{15}					1.00	-0.03	0.04	0.05	0.04
ϕ_{16}						1.00	0.05	-0.08	0.07
ϕ_{17}							1.00	-0.06	0.41
ϕ_{18}								1.00	0.05
ϕ_{19}									1.00

Table 1.6

Correlation Matrix for Middle Camera Distance

	ϕ_1	ϕ_2	ϕ_3	ϕ_4	ϕ_5	ϕ_6	ϕ_7	ϕ_8	ϕ_9	ϕ_{10}
ϕ_1	1.00	0.13	0.01	0.28	0.04	0.34	-0.03	0.16	0.28	0.14
ϕ_2		1.00	-0.07	0.02	-0.12	0.17	-0.11	-0.06	0.01	0.09
ϕ_3			1.00	0.01	0.02	-0.08	0.01	0.03	0.03	0.01
ϕ_4				1.00	0.54	-0.14	-0.15	0.10	-0.07	-0.14
ϕ_5					1.00	-0.38	0.05	0.10	-0.23	0.06
ϕ_6						1.00	-0.11	-0.20	0.55	0.31
ϕ_7							1.00	0.02	-0.05	0.34
ϕ_8								1.00	0.27	-0.02
ϕ_9									1.00	0.21
ϕ_{10}										1.00
ϕ_{11}										
ϕ_{12}										
ϕ_{13}										
ϕ_{14}										
ϕ_{15}										
ϕ_{16}										
ϕ_{17}										
ϕ_{18}										
ϕ_{19}										

Table 1.6 continued.

	ϕ_{11}	ϕ_{12}	ϕ_{13}	ϕ_{14}	ϕ_{15}	ϕ_{16}	ϕ_{17}	ϕ_{18}	ϕ_{19}
ϕ_1	0.13	-0.20	0.09	-0.02	-0.002	0.04	0.76	-0.11	0.36
ϕ_2	-0.01	-0.56	0.06	0.04	0.05	-0.10	0.10	-0.19	0.08
ϕ_3	-0.04	0.19	0.01	-0.01	-0.01	0.004	0.04	-0.02	0.02
ϕ_4	-0.01	0.14	0.22	0.24	0.55	-0.02	0.35	-0.25	-0.12
ϕ_5	-0.07	0.38	0.02	0.02	0.32	0.06	0.34	0.30	-0.34
ϕ_6	0.24	-0.42	0.16	-0.01	-0.16	-0.08	0.14	-0.36	0.74
ϕ_7	-0.02	0.01	-0.01	-0.65	-0.51	0.62	0.05	0.63	-0.08
ϕ_8	0.15	0.22	0.03	0.02	0.03	0.04	0.33	0.05	0.25
ϕ_9	0.35	-0.02	0.13	-0.01	-0.13	-0.01	0.27	-0.18	0.83
ϕ_{10}	0.09	-0.18	0.04	-0.59	-0.50	0.33	0.11	0.38	0.28
ϕ_{11}	1.00	0.01	0.06	0.01	-0.04	0.002	0.14	-0.08	0.40
ϕ_{12}		1.00	-0.04	0.01	0.08	0.10	-0.02	0.23	-0.13
ϕ_{13}			1.00	-0.01	0.37	-0.13	0.08	-0.27	0.16
ϕ_{14}				1.00	0.75	-0.58	-0.05	-0.77	-0.01
ϕ_{15}					1.00	0.57	0.04	-0.70	-0.17
ϕ_{16}						1.00	0.10	0.57	-0.03
ϕ_{17}							1.00	0.07	0.30
ϕ_{18}								1.00	-0.26
ϕ_{19}									1.00

Table 1.7

Correlation Matrix Elements[a]

Matrix Element	Parameter
ϕ_1	r(Si-Si)
ϕ_2	r(Si-C)
ϕ_3	r(C-H)
ϕ_4	< Si-Si-H(1)
ϕ_5	< C-Si-Si
ϕ_6	< Si-C-H
ϕ_7	< C-Si-Si-H(1)
ϕ_8	l(Si-Si)
ϕ_9	l(Si-C)
ϕ_{10}	l[C···C(1,3)]
ϕ_{11}	l(C-H)
ϕ_{12}	l[H···H(1,3)]
ϕ_{13}	l[Si···Si(1,3)]
ϕ_{14}	l[Si···C(1,3)]
ϕ_{15}	l[Si···C(1,4)G]
ϕ_{16}	l[Si···C(1,4)T]
ϕ_{17}	l[Si···H(1,3)]
ϕ_{18}	l(Si···H)
ϕ_{19}	R

[a] Coefficients are given by $\rho_{kl} = (M_x^o)_{kl}[(M_x^o)_{kk}(M_x^o)_{ll}]^{-1/2}$ where (M_x^o) is an element of the zeroth-order error matrix.[14]

with elements proportional to $P(s) \times s^2$, where $P(s)$ is the plateau function in terms of s, was employed in deriving the correlation matrices.

DISCUSSION

The structural parameters derived by a least squares analysis of the composite molecular intensities do not differ greatly from the parameters obtained from the middle distance intensities alone. The C-H bond length is the same for both analyses at 1.114 Å°--the only difference being in the estimated error. The least squares analysis of the middle distance intensities resulted in smaller estimated errors for the bonded distances than the errors from the composite molecular intensity analysis. On the other hand, the nonbonded distances determined from the blended camera distances had lower standard deviations than those of the middle camera distance data. As stated in the Results Section, the 11 cm distance data cannot provide enough information for an accurate conformational determination. The nonbonded distances depend to a large extent on the bond angles and torsions.

In the two least squares analyses, the angles and torsions were determined from the blended data and held constant at these values for the middle distance data analysis. The error estimates for the bond angles and the torsions are lower for the blended intensities for the reasons stated above. Alternatively, the middle distance intensities produced smaller error estimates for the bonded amplitudes of vibration but larger error estimates for the nonbonded amplitudes. The bonded and the non-

bonded amplitudes from the middle camera distance analysis are smaller than the corresponding values determined from the blended data except for the C...C(1,3) amplitude which is the same in both.

The structure reported for tris(trimethylsilyl)silane is a combination of the parameters derived from the two analyses. The bonded distances and amplitudes are those determined from the middle distance data. The bond angles, torsions, and nonbonded distances and amplitudes are those of the blended data analysis. The structural parameters are listed with their estimated standard deviations in Table 1.8.

Several parameters were not varied in the least squares refinement. Initially the Si-H bond length and corresponding amplitude were varied. However the value of the Si-H bond increased with every cycle of the least squares program with an estimated error of ± 0.1 A°. Since the standard deviation was so large and the parameter would not converge, the bond length was frozen at a value reported for Si-H bonds.[13] The bonded amplitude was also held constant.

As stated in the section on the molecular description, the silicon tilt was incorporated into the model to test for bent bonds and to accommodate the intermethyl repulsions between trimethylsilyl groups. The molecular structure did not converge when the tilt angle was allowed to vary. In every case when the parameter was varied by the

Table 1.8

Structural Parameters[a] and Estimated Uncertainties[b] for $[(CH_3)_3Si]_3SiH$ and $[(CH_3)_3Si]_4Si$[c]

Parameter		$[(CH_3)_3Si]_3SiH$	$[(CH_3)_3Si]_4Si$
Si-H(1)	r_g	1.484[e]	----
	l_g	0.127[e]	----
Si-Si	r_g	2.353 ± 0.006	2.361 ± 0.006
	l_g	0.067 ± 0.010	0.065 ± 0.006
Si-C	r_g	1.885 ± 0.002	1.889 ± 0.006
	l_g	0.055 ± 0.005	0.055 ± 0.006
C-H	r_g	1.114 ± 0.010	1.117 ± 0.008
	l_g	0.074 ± 0.010	0.071 ± 0.008
Si-Si-H(1)	Angle	103.9 ± 2.0	----
Si-Si-Si	Angle	114.7 ± 4.0	109.47
C-Si-Si	Angle	110.5 ± 0.8	110.9 ± 1.2
Si-C-H	Angle	109.8 ± 2.1	109.3 ± 3.4
C-Si-Si-H(1)	τ	57.4 ± 4.4	11.0[d] ± 7.2
H-C-Si-Si	τ	0.0[e]	----
Silicon tilt		0.0[e]	----
C···C(1,3)	r_g	3.052 ± 0.018	3.054 ± ----
	l_g	0.105 ± 0.018	0.116 ± 0.018
Si···Si(1,3)	r_g	3.962 ± 0.030	3.855 ± ----
	l_g	0.133 ± 0.022	0.135 ± 0.015
Si···C(1,3)	r_g	3.493 ± 0.018	----
	l_g	0.148 ± 0.020	----

[a] Distances and amplitudes in A°, angles in degrees.

[b] Estimated uncertainties include the effects of both random and systematic errors and are reported as 2σ.

[c] L. S. Bartell, F. B. Clippard, Jr., and T. L. Boates, Inorg. Chem., 9, 2436 (1970).

[d] Angle represents degrees of deviation from T_d symmetry.

[e] Not varied.

program, the estimated standard error was equal to or greater than the deviation of the bond from linearity. With the tilt angle held constant at 0.0°, the structure was finally refined.

The methyl groups were fixed at local C_{3v} symmetry, and no attempt was made to vary their torsional parameter. The three trimethylsilyl torsions were ultimately constrained to be equal. Before the final structural refinement, the trimethylsilyl torsional angles were allowed to vary independently. Two of the groups would consistently rotate in the same direction and to the same extent. The third group rotated in the opposite direction. None of these variations led to convergence of the torsional parameters, and therefore no numerical values will be reported or discussed.

The structural parameters for tris(trimethylsilyl)-silane compare favorably with those of tetrakis(trimethylsilyl)silane. The bonded distances and the bonded amplitudes of vibration for the two molecules are in agreement within the estimated errors although the bond lengths for the tris-substituted silane are smaller than the corresponding lengths in the tetrakis compound. Parameters for $[(CH_3)_3Si]_4Si$ are listed in Table 1.8.

The C-Si-Si and the Si-C-H angles are in excellent agreement between the two molecules. The four tertiary silicons in tetrakis(trimethylsilyl)silane assume a tetrahedral arrangement whereas the Si-Si bonds around the

central silicon in tris(trimethylsilyl)silane can relax without the constraint of the fourth trimethylsilyl group. The Si-Si-H(1) angle is 103.9° ± 2.0° instead of the tetrahedral value. Where the trimethylsilyl torsion reported for $[(CH_3)_3Si]_3SiH$ is 2.6° ± 4.4° from a staggered configuration, the corresponding torsion in $[(CH_3)_3Si]_4Si$ is 11° ± 3.6° from a staggered configuration. Thus in tris(trimethylsilyl)silane, the trimethylsilyl groups are essentially staggered. The deviation from a tetrahedral arrangement at the central silicon in tris(trimethylsilyl)-silane apparently reduces the intermethyl repulsions and eliminates the trimethylsilyl torsion.

The C···C(1,3) distances of 3.052 A° and 3.054 A°, respectively, for the tris and tetrakis substituted silanes show close agreement in the internal geometry of the functional groups. Likewise, the Si-C-H angle is 109.8° ± 2.1° for the tris silane and 109.3° ± 3.4° for the tetrakis silane. The C-Si-Si angles are 110.5° ± 0.8° and 110.9° ± 1.2° for the tris and tetrakis compounds, respectively. The bond lengths and angles indicate essentially the same trimethylsilyl geometry between the two molecules.

Significant structural differences do exist around the central silicon in terms of the central bond angle and the trimethylsilyl torsion. The fourth trimethylsilyl group seems to cause a small strain, increasing the bond lengths slightly. Tris(trimethylsilyl)silane takes advantage of the open space in the vicinity of the silicon-

hydrogen bond to relieve the intermethyl repulsions.

Tri-tert-butylmethane, TTBM, or $[(CH_3)_3C]_3CH$, the hydrocarbon analog of tris(trimethylsilyl)silane, undergoes strain from the large t-butyl groups attached to the tertiary carbon atom. The C-C length of the central carbon to the quaternary carbons is the longest reported for an alkane[15,16] at 1.611 A° ± 0.010 A°. In tris(trimethylsilyl)silane the analogous Si-Si bond is about 50% longer at 2.353 A° ± 0.006 A°. The Si-Si bond is the same within experimental error as that reported for other silanes. While the methyl carbon to tertiary carbon length although slightly long at 1.548 A° ±0.004 A° is more typical of C-C lengths, the methyl groups in each t-butyl group have been forced together as evidenced by the value of 113.0° ± 0.4° for the C_t-C_q-C_m* angle. The corresponding angle in tris(trimethylsilyl)silane is the C-Si-Si angle at 110.5° ± 0.8°.

Bürgi and Bartell[15,16] reported the t-butyl torsion as 10.8° ± 1.0° from a staggered conformation and the methyl groups 18.0° ± 12° from a staggered position. As discussed above, the trimethylsilyl groups within the estimated error are staggered, and the methyl groups constrained to C_{3v} symmetry. Nevertheless, the lack of strain in the silane makes the assumption of staggered methyl groups reasonable.

---

* t = tertiary, q = quaternary, m = methyl.

SUMMARY

The results of this work on tris(trimethylsilyl)-silane show bonded parameters, within experimental error, to be the same as the bonded parameters found for tetrakis-(trimethylsilyl)silane. Tris(trimethylsilyl)silane lacks the torsional twist found in tetrakis(trimethylsilyl)-silane about the central silicon atom because the absence of the fourth functional group gives greater freedom to the tris-substituted molecule to relieve nonbonded repulsions by bond angle bending. Serious strain due to tight packing of the t-butyl groups in TTBM leads to significant distortions in the tetrahedral configurations about the various carbon atoms. The intermethyl repulsions are important in describing the TTBM geometry. On the other hand, the longer Si-Si and Si-C bond lengths in tris(trimethylsilyl)silane place the methyl groups at sufficient separation to make the molecule virtually strain free when compared to smaller, and less crowded, silanes.[11] The Si-Si-H(1) angle at 103.9° ± 2.0° accounts for the largest deviation from a tetrahedral arrangement around the Si and C atoms. On the other hand, the C_q-C_t-H_t angle of 101.6° ± 0.4° in TTBM shows an even larger deviation from the tetrahedral angle.

REFERENCES

1. M. T. Tribble and N. L. Allinger, Tetrahedron, 28, 2147 (1972).

2. H. Bürger and W. Kilian, J. Organometal. Chem., 18, 299 (1969).

3. L. S. Bartell in Physical Methods in Chemistry, 4th Edition, A. Weissberger and B. W. Rossiter, Eds., Interscience, New York, 1973.

4. W. F. Bradford, Doctoral Dissertation, University of Michigan, 1974.

5. L. Schafer, A. C. Yates, and R. A. Bonham, J. Chem. Phys., 55, 3055 (1971).

6. C. Tavard, D. Nicolas, and M. Rouault, J. Chim. Phys., 64, 540, 555 (1967).

7. R. A. Bonham and L. S. Bartell, J. Chem. Phys., 31, 702 (1959).

8. L. S. Bartell, J. Chem. Phys., 23, 1219 (1955).

9. K. Kuchitsu and L. S. Bartell, J. Chem. Phys., 35, 1945 (1961).

10. L. O. Brockway and J. Y. Beach, J. Amer. Chem. Soc., 60, 1836 (1938).

11. L. S. Bartell, F. B. Clippard, Jr., and T. L. Boates, Inorg. Chem., 9, 2436 (1970).

12. Martin Klessinger, Chem. Phys. Lett., 4, 144 (1969).

13. R. W. Kilb and L. Pierce, J. Chem. Phys., 27, 108 (1957).

14. L. S. Bartell and Hsuikang Yow, J. Mol. Structure, 15, 173 (1973).

15. H. B. Bürgi and L. S. Bartell, J. Amer. Chem. Soc., 94, 5236 (1972).

16. L. S. Bartell and H. B. Bürgi, J. Amer. Chem. Soc., 94, 5239 (1972).

PART II. LOW TEMPERATURE INFRARED INVESTIGATION OF IF_7.

ELECTRON DIFFRACTION AND STRUCTURAL INVESTIGATION OF IF_7

Adams, Thompson, and Bartell, investigating the structure of iodine heptafluoride by gas phase electron diffraction, reported a structure which deviates slightly from D_{5h} symmetry.[1] These deviations from D_{5h} symmetry can best be seen in the Fourier sine transform of the composite reduced molecular intensity[2] for IF_7. Figure 1 of Reference 1 shows the experimental curve and the theoretical curve for a D_{5h} structure.

The nonbonded distance region between 2.1 A° and 2.7 A° in the radial distribution function contains a slight misfit of the calculated and the experimental curves. The peak corresponding to the short equatorial fluorine ($F_{eq}\cdots F_{eq}$) nonbonded distance (approximately 2.2 A°) has been moved to a larger internuclear distance relative to a D_{5h} reference structure. On the other hand, the peak corresponding to the axial-equatorial fluorine ($F_{ax}\cdots F_{eq}$) nonbonded distance (approximately 2.5 A°) has been moved to a smaller internuclear distance relative to a D_{5h} reference structure. Furthermore, the $F_{ax}\cdots F_{eq}$ peak has been skewed, relative to the reference, indicating the shortening of some axial-equatorial distances and the lengthening of other $F_{ax}\cdots F_{eq}$ distances.

While the deviations of iodine heptafluoride from D_{5h} symmetry are small, they cannot be ignored. A rigid D_{5h} structure is not consistent with the experimental

diffraction intensities. Thus the problem is one of finding a geometric model which incorporates the displacements from a D_{5h} structure in the nonbonded distance region between 2.1 A° and 2.7 A°.

Adams, Thompson, and Bartell found that the coupling of vibrations of different symmetry modes could explain the distribution of nonbonded distances in the experimental radial distribution function. If the equatorial fluorines in IF_7 undergo a displacement along the $e_2"$ symmetry coordinate, each short $F_{eq}\cdots F_{eq}$ nonbonded distance is lengthened relative to the D_{5h} reference. The $F_{eq}\cdots F_{eq}$ lengthening is apparent in Figure 2.1 which depicts the D_{5h} bending symmetry coordinates for IF_7. An $e_2"$ deformation in IF_7 lengthens some of the axial-equatorial distances but shortens others. However the displacement of the fluorine atoms along an $e_2"$ coordinate alone cannot produce the skewing of the $F_{ax}\cdots F_{eq}$ peak in the f(r). That is to say, independent harmonic vibrations cannot accommodate the experimental diffraction intensities.

The coupling of vibrations along different symmetry coordinates requires the inclusion of higher order anharmonic terms in the molecular force field. The most significant anharmonic contribution would come from the term, $F_{iij}(S_i)^2(S_j)$, where S_i and S_j represent the bending symmetry coordinates and F_{iij} is the corresponding cubic force constant. The proper coordinates to skew the axial-equatorial peak are those which affect the axial and equa-

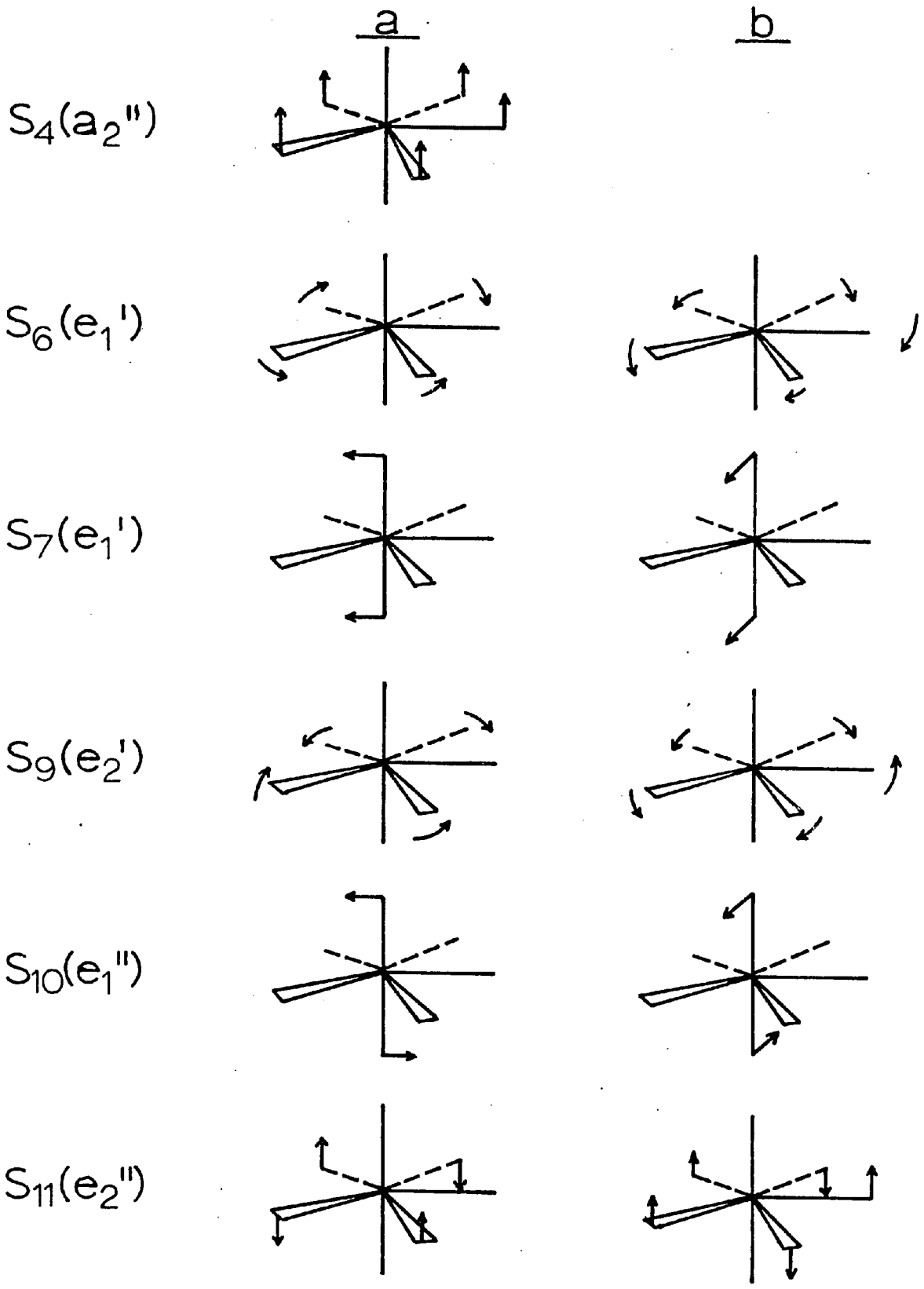


Figure 2.1. D_{5h} Bending Coordinates.

torial nonbonded distances. This requires at least one of the coordinates to be an axial bend or an equatorial bend. Of the force field terms meeting the prescribed criterion, $(e_2")^2(e_1')$, $(e_1')^2(e_2')$, and $(e_1")^2(e_2')$, only the $(e_2")^2(e_1')_{axial}$ contains the symmetry coordinates capable of giving the proper skew to the 2.5 A° peak. Two conformations which maintain C_2 and C_s symmetry, respectively, of iodine heptafluoride deformed along the $e_2"$ and the e_1' coordinates are depicted in Figure 2.2.

PSEUDOROTATION IN IF_7

Adams subjected several geometric models to a least squares analysis of the IF_7 diffraction intensities. The C_2 and the C_s structures can be described in terms of an angular displacement of the equatorial fluorines, α_{eq}, and the axial fluorine bend, α_{ax}, from a D_{5h} reference structure. The standard deviation of the composite molecular intensity for the D_{5h} model is 1.792 parts per thousand (ppt) whereas the standard deviations for the C_2 and the C_s conformers are essentially equal with values of 1.345 ppt and 1.350 ppt, respectively. An equal mixture of C_2 and C_s conformers has a standard deviation of 1.347 ppt.

Adams, Thompson and Bartell proposed for IF_7 a model of dynamic pseudorotation in which the molecule passes through ten alternating C_2 and C_s conformations in one pseudorotational cycle. The model of pseudorotation for

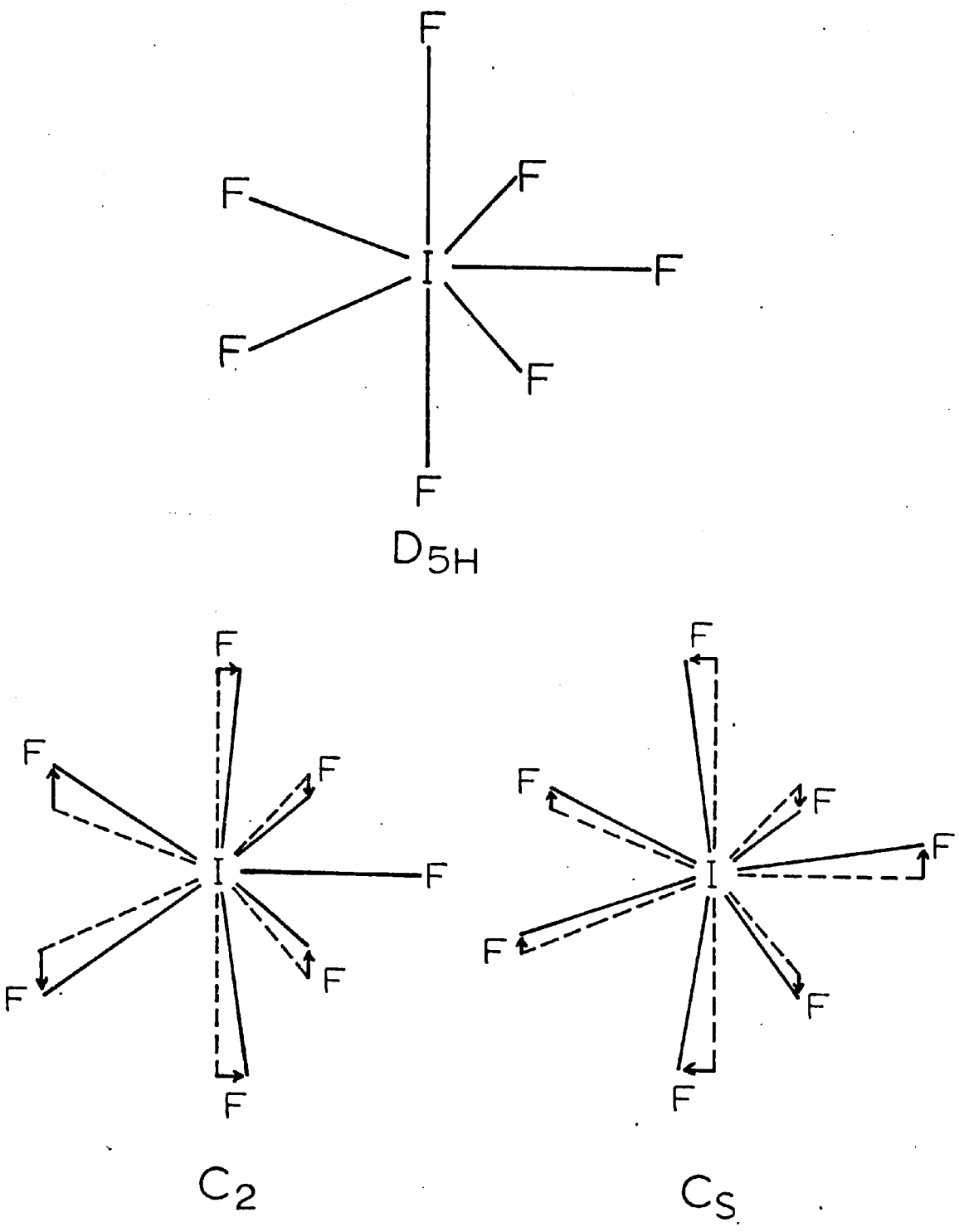


Figure 2.2. Conformations for IF_7.

IF_7 is analogous to the pseudorotational model which Pitzer proposed for cyclopentane.[3] The $e_2"$ vibration of the equatorial fluorines in iodine heptafluoride corresponds to the puckering of the five-carbon ring in cyclopentane. IF_7 has the added feature of the e_1' axial fluorine bend coupled to the equatorial fluorine bend.

The mathematical expressions describing the angular displacements of the equatorial and axial fluorine atoms have already been discussed by Adams, Thompson, and Bartell. The equatorial angular displacement is a function of the maximum bend and the phase of the maximum displacement. In order to couple the $e_2"$ and e_1' vibrations in the pseudorotation model, a phase relationship based on the static C_2 and C_s models was devised. It is important to note that pseudorotation is not a true rotation but a vibration with an associated phase angle rotation.

The structural parameters are essentially independent of the phase angles.[1] The C_2 and C_s structures and conformations intermediate between the C_2 and the C_s configurations cannot be distinguished. In short, electron diffraction by itself cannot determine whether iodine heptafluoride exists in a variety of conformers deformed from a D_{5h} reference geometry or whether the molecule undergoes pseudorotation.

Additional experimental evidence supporting the distorted geometry of IF_7 has been reported.[4] A molecular beam of IF_7 was focused by an inhomogeneous electric field.

At 20°C IF_7 was observed to be nonpolar but exhibited polar components as the temperature was lowered. The intensity of the polar components increased with decreasing temperature. The focusing of a beam of rigid, polar molecules should be independent of temperature, but rigid nonpolar molecules should not focus at all.

SPECTROSCOPIC INVESTIGATIONS OF IODINE HEPTAFLUORIDE

Gas phase infrared and Raman spectra of iodine heptafluoride were recorded by Claassen, Gasner and Selig.[5] Previous gas phase spectra of IF_7 reported by Lord[6] were shown by Bartlett and Levchuk to contain significant amounts of IOF_5.[7] The infrared fundamentals of IF_7 are presented in Table 2.1 along with the vibrational fundamentals of IF_5 and IOF_5 for comparison.

Claassen assigned the infrared and Raman frequencies of IF_7 with D_{5h} selection rules. His Raman and infrared assignments appear in Table 2.2. The odd feature of this assignment is that the e_1'' bend is given the value of 510 cm^{-1} whereas the e_2' stretch is assigned a frequency of 310 cm^{-1}. In spite of a bending vibration having a higher frequency than a stretching vibration, all combination bands are binary and obey the D_{5h} selection rules.

Eysel and Seppelt obtained gas phase Raman and infrared spectra of iodine heptafluoride. Except for the 520 cm^{-1} and the 552 cm^{-1} combinations reported by Claassen,

Table 2.1

Infrared Fundamental Vibrations of IF_7, IOF_5, IF_5

(Gas Phase)

IF_7[a]	IF_5[b]	IF_5[c]	IOF_5[d]
257		309	275
	318	350	
365		370	342
	372	565	
425		610	360
	595	701	
670		719	369
	640	1025	
746			640
	710		
			680
			710
			927

[a] Howard H. Claassen, Earl L. Gasner, and Henry Selig, J. Chem. Phys., 49, 1803 (1968).

[b] G. M. Begun, W. H. Fletcher, and D. F. Smith, J. Chem. Phys., 42, 2236 (1965).

[c] Solid phase (-100°C); R. J. Gillespie and H. J. Chase, J. Chem. Phys., 47, 1071 (1967).

[d] D. F. Smith and G. M. Begun, J. Chem. Phys., 43, 2001 (1965).

Table 2.2

Vibrational Assignments for IF_7

	Frequency			Eysel and	
	R	IR	Claassen	Seppelt	Bernstein
ν_1	676		a_1'	a_1'	a_1'
ν_2	635		a_1'	a_1'	a_1'
ν_3		670	a_2''	a_2''	a_2''
ν_4		365	a_2''	e_1'	a_2''
ν_5		746	e_1'	e_1'	e_1'
ν_6		425	e_1'	e_1'	e_1'
ν_7		257	e_1'	a_2''	e_1'
ν_8	510		e_1''	e_2'	e_2'
ν_9	352		e_2'	e_2'	e_2'
ν_{10}	310		e_2'	e_1''	e_1''
ν_{11}	- -	- -			

they reported essentially the same frequencies as Claassen. In addition to Claassen's combination band frequencies, Eysel and Seppelt reported two bands at 947 cm^{-1} and 990 cm^{-1}. These peaks are not obvious in Claassen's spectra although the bands may be too weak to be seen. Unfortunately, Eysel and Seppelt published only a portion of their spectrum from 250 cm^{-1} to 750 cm^{-1}, preventing a comparison with other spectra. Eysel and Seppelt assigned the frequencies on the basis of D_{5h} selection rules and in fact selected Claassen's frequency values over their own.

Eysel and Seppelt reassigned four frequencies, two of which were the previously mentioned e_1'' bend and the e_2' stretch. They switched the assignment made by Claassen for the bend and the stretch and also switched the assignment for the 365 cm^{-1} vibration with that of the 257 cm^{-1} band. They made the latter change on the basis of the band shape of the 257 cm^{-1} peak, claiming that it is a perpendicular band and therefore cannot be an a_2'' vibration.

Several of the combinations violate the selection rules in the Eysel and Seppelt assignment. The 830 cm^{-1}, 947 cm^{-1}, and 1177 cm^{-1} bands are of the e_2'' species which is infrared and Raman inactive. Since Claassen did not assign the 837 cm^{-1} frequency and did not report the 947 cm^{-1} peak, the 1177 cm^{-1} absorption is considered for comparison of the assignments. In attempting to keep all combinations binary and spectroscopically allowed, Claassen made his unusual assignment of the bend and stretch

vibrations.

A third assignment of Claassen's gas phase frequencies for IF_7 was made by Bernstein.[8] Bernstein disagrees with Eysel and Seppelt in their reassignment of the e_1' and a_2'' modes. Rather, Bernstein supports Claassen's assignment of the 365 cm^{-1} peak as the a_2'' vibration and the 257 cm^{-1} peak as the e_1' vibration. Bernstein points out that Eysel and Seppelt assigned the frequencies based on band contours of a static D_{5h} model and that they ignored the strong coupling of the e_2'' mode with the e_1' mode in the pseudorotating model, which may not have the same band contours as a static D_{5h} model.

Bernstein agrees with Eysel and Seppelt in their assignment of the 510 cm^{-1} peak to the e_2' stretch and the 310 cm^{-1} peak to the e_1'' bend. As stated earlier, this assignment leads to selection rule violations for the 1177 cm^{-1} combination band provided of course that all combinations are binary. In the pseudorotating model, Bernstein's assignment could be valid if the 1177 cm^{-1} combination band (e_2'' in Bernstein's assignment) couples with the pseudorotation mode of e_2'' symmetry.

The foregoing remarks point out the controversy surrounding the gas phase spectra of IF_7 and for that matter, the molecule itself. While Bernstein's assignment is inconsistent with D_{5h} selection rules for strictly binary combinations of a static model, his assignment is accepted

in this text and will be the basis for the spectroscopic investigation of this work. The static D_{5h} model selection rules can be extended to the pseudorotating model of IF_7 if and only if the strong coupling between the e_2'' and e_1' modes and the effects of such a coupling are kept in mind.

MATRIX ISOLATION INVESTIGATION OF IODINE HEPTAFLUORIDE

While the electron diffraction analysis failed to differentiate between a static or dynamic geometric model for iodine heptafluoride, the possibility of a spectroscopic solution requires a description of the pseudorotational energy levels. Pitzer solved the Schrödinger equation for his pseudorotating cyclopentane model in terms of the orthogonal coordinates, q and ϕ. The details of his procedure are adequately covered in Reference 3. Briefly, however, Pitzer separated the two-dimensional pseudorotation problem into two one-dimensional problems--one of simple vibration and one isomorphous with rotation. The energy levels for the pseudoradial coordinate, q, are those of the harmonic oscillator. The rigid rotor-in-a-plane energy levels describe the energy term for the pseudoangular coordinate, ϕ.

For consistency, the notation of Jacob and Bartell[9] has been adopted. Their method is analogous to Pitzer's method but uses as out-of-plane displacements the out-of-plane angles instead of the linear vertical displacements.

The maximum angular displacement, α^o, for IF_7 measured by electron diffraction is related to Pitzer's coordinate, q, as:

$$q = (5/2)^{1/2}\ \alpha^o r(I\text{-}F_{eq}) \qquad (1)$$

where $r(I\text{-}F_{eq})$ is the experimentally determined $r_g(O)$ bond length. The energy expression for the pseudorotation levels is:

$$E_{v,m} \simeq E_v(q) + E_m(\phi) \qquad (2)$$

$E_v(q) = (v + 1/2)h\nu_q$ is the harmonic oscillator expression for the pseudoradial term where ν_q is the pseudorotation frequency. For D_{5h} selection rules, ν_q is an e_2'' species which is both infrared and Raman inactive. The pseudoangular energy term is $E_m = m^2h^2/(8\pi^2M_Fq_e^2)$ where M_F is the fluorine mass, m = 0, ± 1, ± 2 .... and q_e is the value of q at the potential energy minimum. The assumption is made that the mean amplitude, $\langle\alpha^o\rangle$, measured by electron diffraction is very nearly equal to α_e^o, the minimum energy value. For iodine heptafluoride, the value of $h^2/8\pi^2M_Fq_e^2 \simeq 5\ cm^{-1}$.

While the e_2'' vibration is itself Raman and infrared inactive, the strong coupling of the e_2'' and the e_1' species should enable the e_2'' overtones to be infrared active. Furthermore, the combination bands between the pseudoradial and pseudoangular terms should also be infrared

active. Durig and Wertz reported the infrared pseudorotational bands in cyclopentane.[10] With the success of the pseudorotation model for cyclopentane, a spectroscopic examination of iodine heptafluoride to search specifically for the pseudorotation bands seemed worth the undertaking.

In order to look for spectroscopic evidence of pseudorotation in IF_7, a preliminary discussion of the possible frequencies is desirable. Bernstein's assignment of the gas phase infrared frequencies[8] offers a starting point. With the pseudorotational model postulated in accord with small displacements from a D_{5h} reference geometry, the D_{5h} point group provides the selection rules for spectroscopic activity. Table 2.3 presents a compilation of the e_2'' combinations with all the other D_{5h} symmetry species. Combinations of the e_2'' mode with known iodine heptafluoride infrared and Raman fundamentals have been marked. Of the relevant symmetry combinations, only two combinations between different symmetry species are formally infrared active. These are $e_1'' \times e_2''$ and $e_2' \times e_2''$. As stated earlier, the $e_2'' \times e_2''$ overtone is also formally infrared active.

The pseudoradial frequency, ν_q, is identified with the inactive e_2'' frequency designated as ν_{11} in the gas phase frequency assignments. The pseudoangular energy levels are $E_m = m^2 B_{ps}$ where $m = 0, \pm 1, \pm 2 \ldots$ and $B_{ps} = h^2/8\pi^2 M_F q_e^2 \approx 5\ cm^{-1}$ for IF_7 and should be capable of modulating the pseudoradial frequency. Such transitions where $\Delta v = 1$ and $\Delta m = 1$ would appear as pseudorotational fine

Table 2.3

Combinations of e_2'' with D_{5h} Symmetry Species[b]

Combination	Resultant	Activity
$a_1' \times e_2'' = e_2''$		Inactive[a]
$a_1'' \times e_2'' = e_2'$		R
$a_2' \times e_2'' = e_2''$		Inactive
$a_2'' \times e_2'' = e_2'$		R[a]
$e_1' \times e_2'' = e_1'' + e_2''$		R[a]
$e_1'' \times e_2'' = e_1' + e_2'$		IR,R[a]
$e_2' \times e_2'' = a_1'' + a_2'' + e_1''$		IR,R[a]
$e_2'' \times e_2'' = a_1' + e_1'$		IR,R

[a] Indicates possible combinations with IR or Raman fundamentals of IF_7.

[b] Compiled from tables in Gerhard Herzberg, Infrared and Raman Spectra of Polyatomic Molecules, D. Van Nostrand Company, Inc., Princeton (1945) and E. Bright Wilson, Jr., J. C. Decius and Paul C. Cross, Molecular Vibrations, McGraw-Hill Book Company, New York (1955).

structure on ν_q. These fine structure lines would have frequencies on the order of $\nu_q \pm m^2\ 5\ cm^{-1}$. The pseudo-angular overtones with the $\Delta m = 2$ selection rule are also expected to have infrared activity.

As for the combination bands, there are two Raman fundamentals at 352 cm^{-1} and 510 cm^{-1}, respectively, assigned as e_2' vibrations. So, for example, the pseudo-radial and e_2' combination might be located in the vicinity of 352 $cm^{-1} \pm \nu_q$. Likewise the pseudoangular component might modulate the e_2' frequencies as, for example, 352 $cm^{-1} \pm m^2\ B_{ps}$. The argument can be carried further for the other combinations. In each case, the fundamental frequency observed in the infrared or Raman region may combine with either the pseudoradial or the pseudoangular component to form a symmetry allowed infrared transition.

EXPERIMENTAL

The search for pseudorotation bands in iodine heptafluoride requires highly resolved spectra of a reactive substance. IF_7* is a superb fluorinating agent, decomposes readily on metal surfaces, reacts with glass to form SiF_4, and spontaneously decomposes in the presence of water to IOF_5 and HF.[7] The method of low temperature matrix isolation was adopted as the best way to attack the problem of pseudorotation in IF_7.

The isolation of a substance in an inert matrix permits the recording of spectra otherwise unattainable. The method was developed for observation of reactive molecules and radicals[12,13] and has been used successfully to investigate a number of different chemical species.[14] Since the inert matrices are maintained at low temperatures (T<30K), sharply resolved spectra can be obtained.[15]

The underlying principle of low temperature matrix isolation is to secure molecules or radicals in lattice sites or matrix "holes" at reduced temperatures of liquified gases like hydrogen or helium. Noble gases are often selected as matrix material because they are for the most

---

* IF_7 can be synthesized by adding a two-fold excess of fluorine to distilled IF_5 for one hour at 200°C. The unreacted fluorine can be removed by vacuum distillation with the resulting IF_7 free of any IOF_5 contamination.[11]

part chemically inert and are essentially transparent to infrared radiation. The low temperature of the liquified gas refrigerant insures the rigidity of the matrix and prevents diffusion of the sample molecules. In the ideal case there are no molecular aggregates of the sample and no sample-matrix interactions.

From the experimental standpoint, the sample and matrix material are sprayed onto a support window which is transparent to infrared radiation and which is held at a sufficiently low temperature to condense both the sample and the matrix material. The matrix formation is extended over a period of several hours to insure adequate isolation of the sample molecules. Suitable isolation is achieved when the mole ratio of matrix material to active substance, M/A, is greater than 100.[16] Prior to matrix formation, the sample and matrix material may be mixed in a single vessel and sprayed onto the cold window through one nozzle. Greater flexibility in regulating the matrix formation and in controlling the M/A value can be achieved by condensing the sample and the matrix substance onto the window from two separate nozzles.

The experimental system for low-temperature matrix isolation spectroscopy was designed and constructed by Dr. Jerry Current. A cryostat with its associated infrared cell was mounted on a mobile rack, complete with two independent vacuum lines. In this way the entire assembly could be moved into position with the low temperature cell

in the sample compartment of a Beckman IR-12 spectrometer. Since the cryostat made closing the sample compartment door impossible, the only modification to the spectrometer was a sheet of plastic to seal the sample compartment which was continuously flushed with dry nitrogen gas. One of the vacuum systems evacuates the cryostat and infrared cell while the other evacuates the sample and matrix introduction system. The separate vacuum lines could be interconnected but were usually operated independently. Both vacuum lines were capable of attaining 10^{-6} torr.

The cryostat was manufactured by Sulfrian Cryogenics of Rahway, New Jersey, and is depicted (not to scale) in Figure 2.3. The innermost chamber holds approximately five liters of refrigerant and is shielded by a second chamber which can be filled with liquid nitrogen. The intervening spaces between the refrigerant vessels and the outer cryostat wall are evacuated.

The spectroscopic cell, Figures 2.3 and 2.4, is mounted at the base of the cryostat and is evacuated through the cryostat. The cell is made of stainless steel and has four circular openings over which windows may be secured with rubber O-rings and brackets. Windows may be changed during an experiment by rotating the cell which is mounted against a ball bearing race. For the investigation on iodine heptafluoride, two of the four ports were sealed with stainless steel plates. Cesium iodide windows which are transparent in the infrared region down to 240

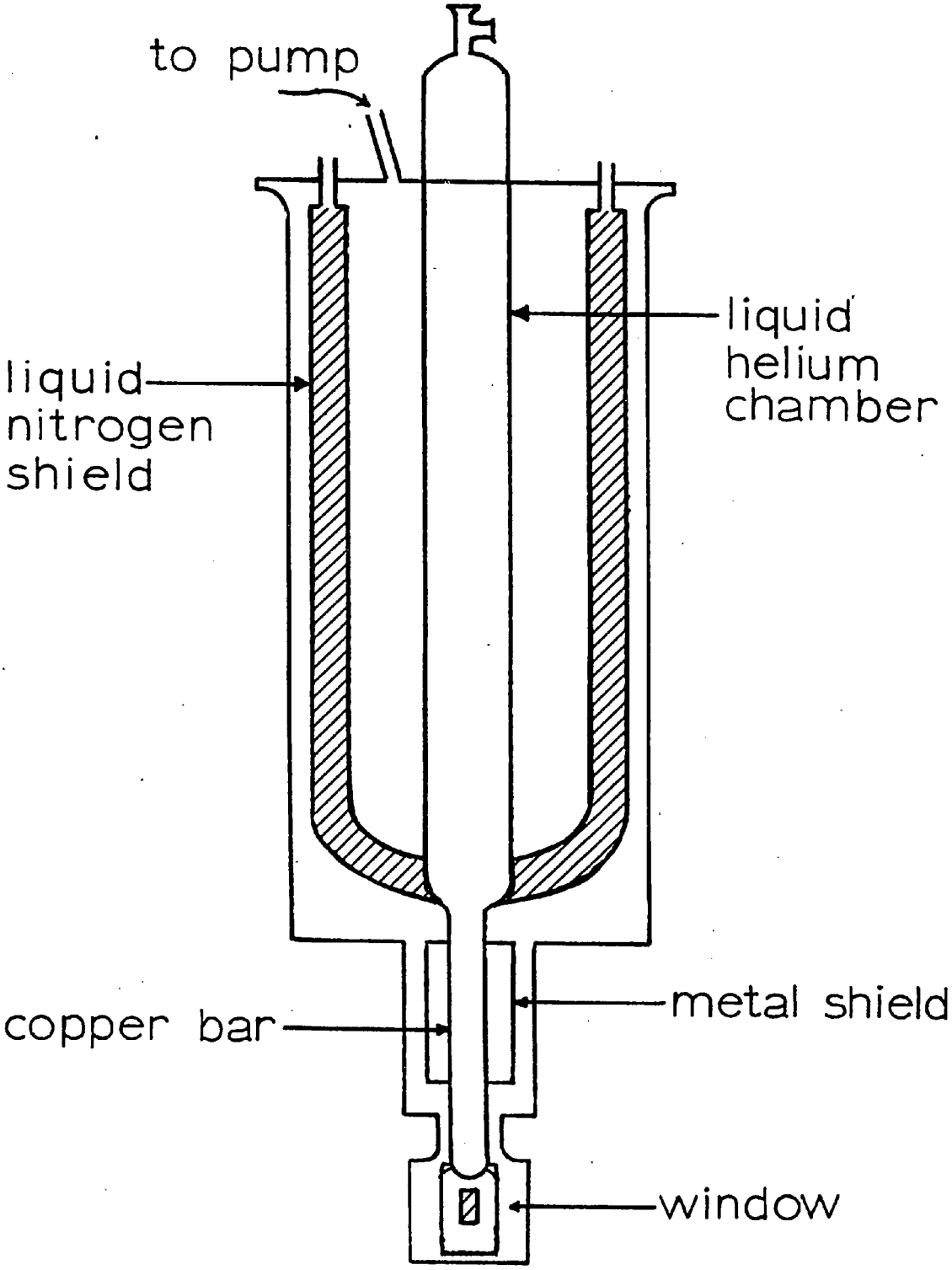
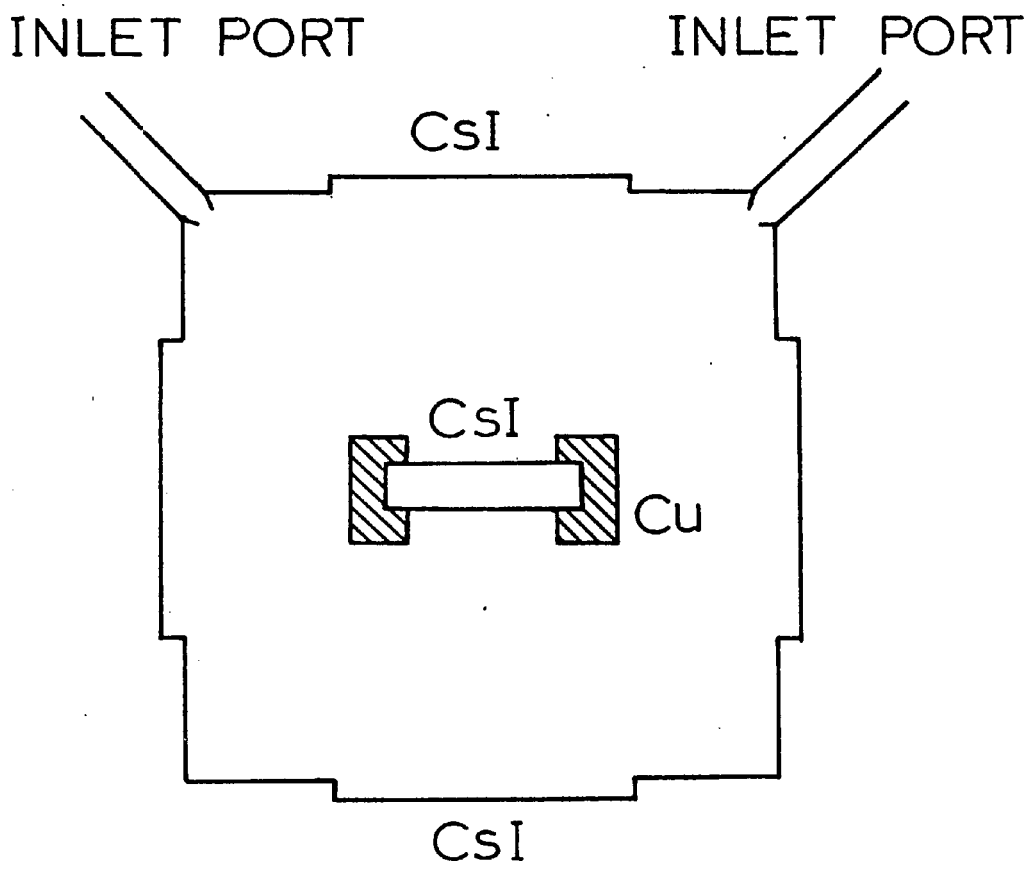


Figure 2.3. Cryostat and IR Cell.



IR CELL

Figure 2.4.

cm^{-1} covered the remaining two cell ports. The entire external cell assembly slips onto the bottom of the cryostat, around a hollow copper bar. The bar in turn is sealed to the base of the cryostat with an indium gasket and is filled with liquid helium from the inner cryostat chamber. Attached to the other end of the copper bar is a 4 x 2 cm cesium iodide window which supports the matrix. Indium gaskets between the CsI window and the copper brackets provide excellent thermal contact.

Two small nozzles located on adjacent corners of the spectroscopic cell and directed toward the matrix support window serve as gas inlet ports for the sample and matrix material, respectively. High purity gases for the matrices were transferred to several two-liter glass bulbs through a liquid nitrogen cold trap to remove water vapor. A small cylinder of iodine heptafluoride* (98% pure) was connected through a Nupro brand metering valve directly to the cryostat cell sample port. The IF_7 introduction line was made of Monel and stainless steel. A separate metal line permitted the cryostat and glass vacuum line to be bypassed during the removal of IF_7 from the system. All interconnections of the sample introduction subassembly were made with Swagelock fittings which do not require stopcock grease because IF_7 reacts with hydrocarbon

---

* Purchased from Research Organic/Inorganic Chemical Corporation, Sun Valley, California.

greases.

For each experiment all three CsI windows were cleaned and polished with 95% ethanol. Both cryostat vessels were precooled with liquid nitrogen. After the inner vessel had been cleared of all nitrogen by flushing with dry helium gas, the chamber was filled with liquid helium. A double-walled evacuated transfer tube was employed to fill the cryostat from a liquid helium Dewar. The transfer tube was flushed with dry helium gas to prevent solid plugs of air from forming in the transfer line.

Certain procedures were instituted to introduce a pure sample of iodine heptafluoride into the cell. With the metering valve closed, the metal introduction line was pressurized with IF_7. The gaseous iodine heptafluoride was allowed to react in the metal line for a minimum of thirty minutes after which the sample introduction line was evacuated through the bypass. This technique known as "seasoning" coats the metal surfaces with nonvolatile fluorides which retard the further decomposition of IF_7 when a fresh sample is passed through the line.

The flow of IF_7 into the spectroscopic cell was controlled by the metering valve and by cooling several loops of the introduction line with a Dry Ice-acetone slush bath. Matrix gas flow was monitored by measuring the pressure drop in the vacuum line. A full charge of liquid helium would maintain the matrix window at liquid helium temperature for approximately eight hours as long as the

vacuum in the entire cryostat remained at 1×10^{-6} torr.

ANALYSIS OF DATA

Infrared spectra of solid samples of IF_7 condensed at liquid nitrogen and at liquid helium temperature, respectively, and IF_7 isolated in matrices of argon, nitrogen, and xenon at liquid helium temperature were recorded on a Beckman IR-12 spectrometer. The spectrometer has a resolving power of 0.25 cm^{-1} at 1000 cm^{-1}. The instrument was operated under normal conditions for obtaining the best possible resolution while maintaining a high signal to noise ratio.

Since the iodine heptafluoride corroded the cesium iodide windows during the experiments, the windows were always polished with a stretched chamois soaked in 95% ethanol. Background spectra of the windows at room temperature and at the reduced operating temperature were taken to check for impurities adhering to the window surfaces. The temperature of the matrix support window was monitored with an iron-constantan thermocouple imbedded into the CsI window and a Keithley digital voltmeter. A water-ice bath served as the thermocouple reference.

Each matrix was deposited onto the window over a period of several hours to insure good sample isolation. However, the matrices were not annealed. Several turns of nichrome resistance wire were wrapped about the copper bar

to heat the window by passing a low current through the wire. The uniformity of heating was not measurable or reproducible. Besides, the possibility of the IF_7 diffusing through the matrix to form aggregates did not seem worth any of the advantages of annealing the matrix.

Matrix formation was monitored by scanning the most intense peaks with the spectrometer. When the strongest absorption registered approximately 90% of the transmittance scale, the matrix deposition was stopped. A complete scan of the infrared region from 250 cm^{-1} to 4000 cm^{-1} was made followed by numerous scans of the fundamental region of IF_7 at various spectrometer settings to achieve the best resolution. Observed vibrational frequencies were checked against the spectra of Claassen and the vibrational assignment of Bernstein. Spectroscopic frequencies of IF_5 and IOF_5 were examined for impurity bands in the spectra.

RESULTS

IF_7 in an Argon Matrix.

The spectrum of iodine heptafluoride isolated in an argon matrix at liquid helium temperature is presented in Figure 2.5. Four observed absorptions are listed in Table 2.4. Two peaks, which appeared in the background spectrum of the windows, are included as dotted portions of the spectrum.

While the gas phase fundamental at 365 cm^{-1} has shifted down to 353 cm^{-1} in the matrix spectrum, the 425 cm^{-1} fundamental did not change frequency. The strong gas phase absorption at 670 cm^{-1} underwent a modest shift to 669 cm^{-1}. The 755 cm^{-1} peak in the matrix corresponds to the 746 cm^{-1} absorption in the gas phase spectrum. Such frequency differences between gas phase and solid phase spectra are not uncommon.[17] Although the 257 cm^{-1} fundamental does not appear in the matrix spectrum, this fundamental is a weak absorption and its absence is not surprising.

The absorption intensities are small for this spectrum with the base line dropping off rapidly with increasing frequency. The ratio of argon to IF_7, M/A, is high for this particular spectrum. The absence of the 927 cm^{-1} peak corresponding to the iodine-oxygen stretch indicates that the sample is free of IOF_5.

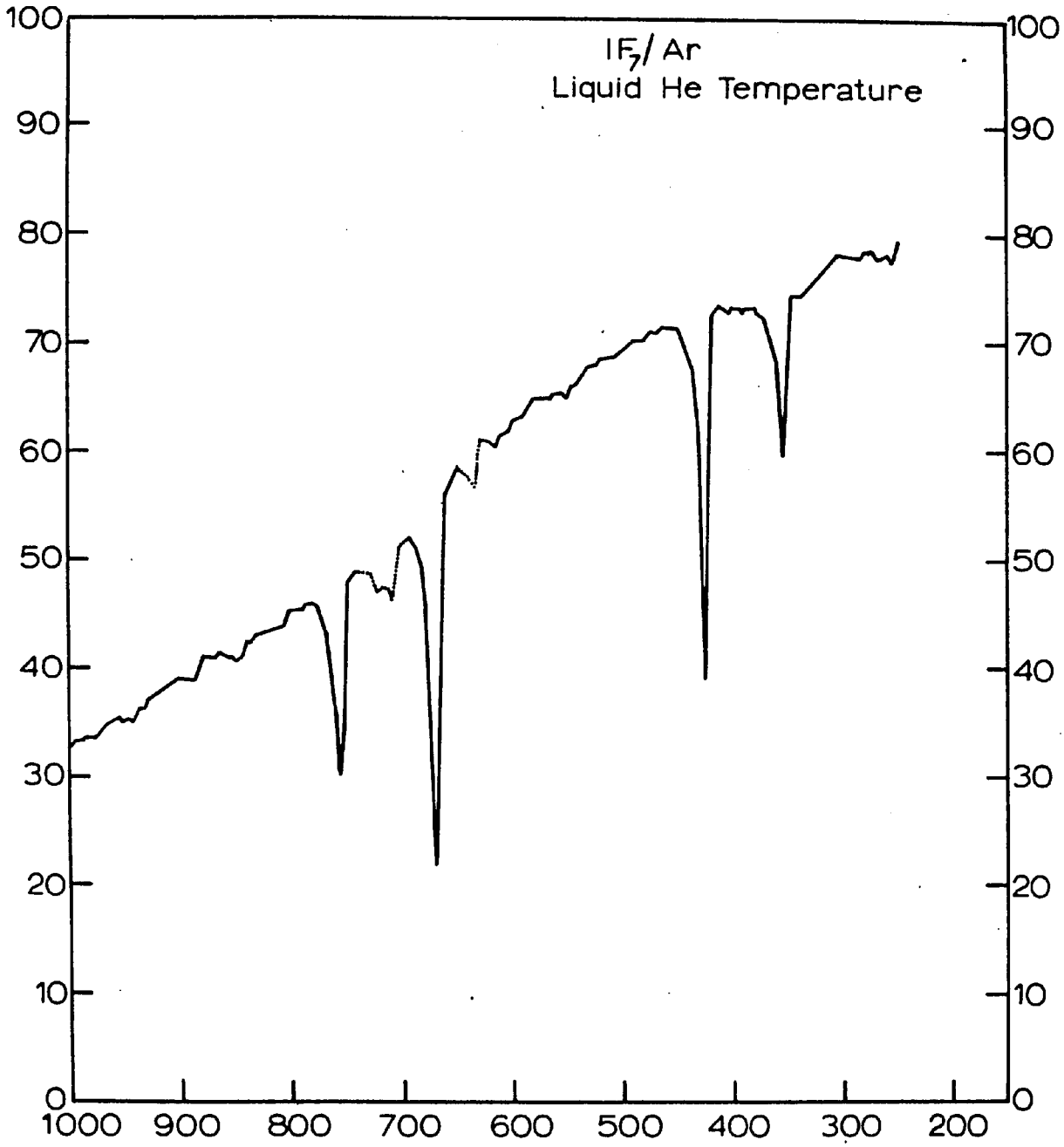

IF7/ Ar
Liquid He Temperature
100
90
80
70
60
50
40
30
20
10
0
1000
900
800
700
600
500
400
300
200

Figure 2.5.

Table 2.4

IF_7/Ar Liquid Helium Temperature

Observed IR Absorptions[a]

353
425
669
755

[a] Frequencies in cm^{-1}.

Table 2.5

Solid IF_7 Liquid Nitrogen Temperature

Observed IR Absorptions[a]

256
346
368
418[b]
663
672
752
768

[a] Frequencies in cm^{-1}.

[b] Peak off recorder chart.

Solid IF_7 at Liquid Nitrogen Temperature

The spectrum of solid IF_7 at liquid nitrogen temperature which appears in Figure 2.6 shows strong intensities with broader peaks than the absorptions recorded for the IF_7/Ar spectrum. As previously stated, there is a certain degree of frequency shifting between the gas phase and solid phase spectra. Observed frequencies are presented in Table 2.5.

The weak transition of 257 cm^{-1} in the gas phase is present in the spectrum at 256 cm^{-1}. The remaining fundamentals are split with the exception of the 425 cm^{-1} gas phase peak which went off scale. So there is no way to tell if this absorption is also split. Peaks which were recorded in the background spectrum are reproduced as dotted portions of the solid IF_7 spectrum.

Two small peaks appear in the solid IF_7 spectrum at 628 cm^{-1} and at 710 cm^{-1}. These features are just visible in Claassen's gas phase spectra although he does not assign the two frequencies. There is no evidence of an absorption at 927 cm^{-1} and consequently IOF_5 is not present as a contaminant.

IF_7 in a Xenon Matrix

The spectrum of IF_7 isolated in a Xenon matrix at liquid helium temperature is presented in Figure 2.7. The

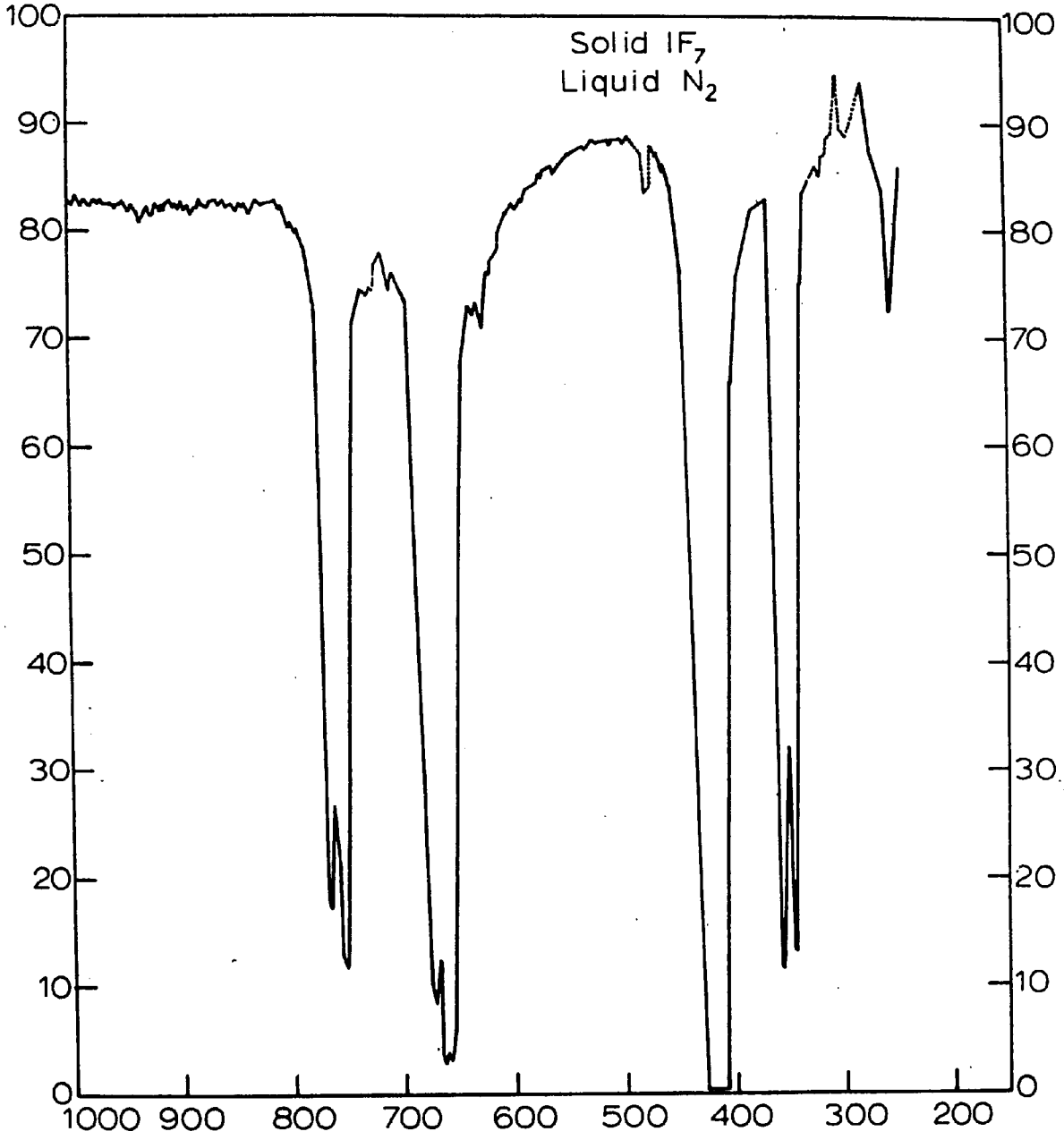

Solid IF_7
Liquid N_2
100
90
80
70
60
50
40
30
20
10
0
1000 900 800 700 600 500 400 300 200

Figure 2.6.

frequencies are listed in Table 2.6 with the five IF_7 fundamentals marked. The remaining frequencies which have counterparts in the IOF_5 gas phase spectrum[18] have been attributed to IOF_5. Certain frequency shifts have occurred although the numerical values are not the same as in the previously tabulated spectra.

Three frequencies, which have not yet been reported for IOF_5, at 549 cm^{-1}, 571 cm^{-1}, and 779 cm^{-1} have been assigned as combination bands of three IOF_5 fundamentals--ν_9, ν_{10}, and ν_{11}. For the 549 cm^{-1} band, the $\nu_{10} + \nu_{11}$ = 342 cm^{-1} + 205 cm^{-1} = 547 cm^{-1} transition is allowed. The 571 cm^{-1} band may be assigned as $\nu_9 + \nu_{11}$ = 369 cm^{-1} + 205 cm^{-1} = 574 cm^{-1} while the 779 cm^{-1} peak is $\nu_9 + 2\nu_{11}$ = 369 cm^{-1} + 2 x 205 cm^{-1} = 779 cm^{-1}. The frequency differences, which are small, are due to the gas phase values assigned to solid phase spectra.

The bands at 536 cm^{-1} and 541 cm^{-1} do not have corresponding peaks in the gas phase spectra. Combinations of IOF_5 fundamentals could not be found for these two bands which are left unassigned. However, it is important to note that the four bands--528 cm^{-1}, 536 cm^{-1}, 541 cm^{-1}, and 549 cm^{-1}--appear only in spectra in which IOF_5 is an obvious impurity. The 528 cm^{-1} peak might be the same peak as Claassen reported at 520 cm^{-1} although Claassen did not assign it. On the other hand, the 528 cm^{-1} peak does not appear unless the 927 cm^{-1} absorption is evident. The intense peak at 927 cm^{-1} indicates severe contamination

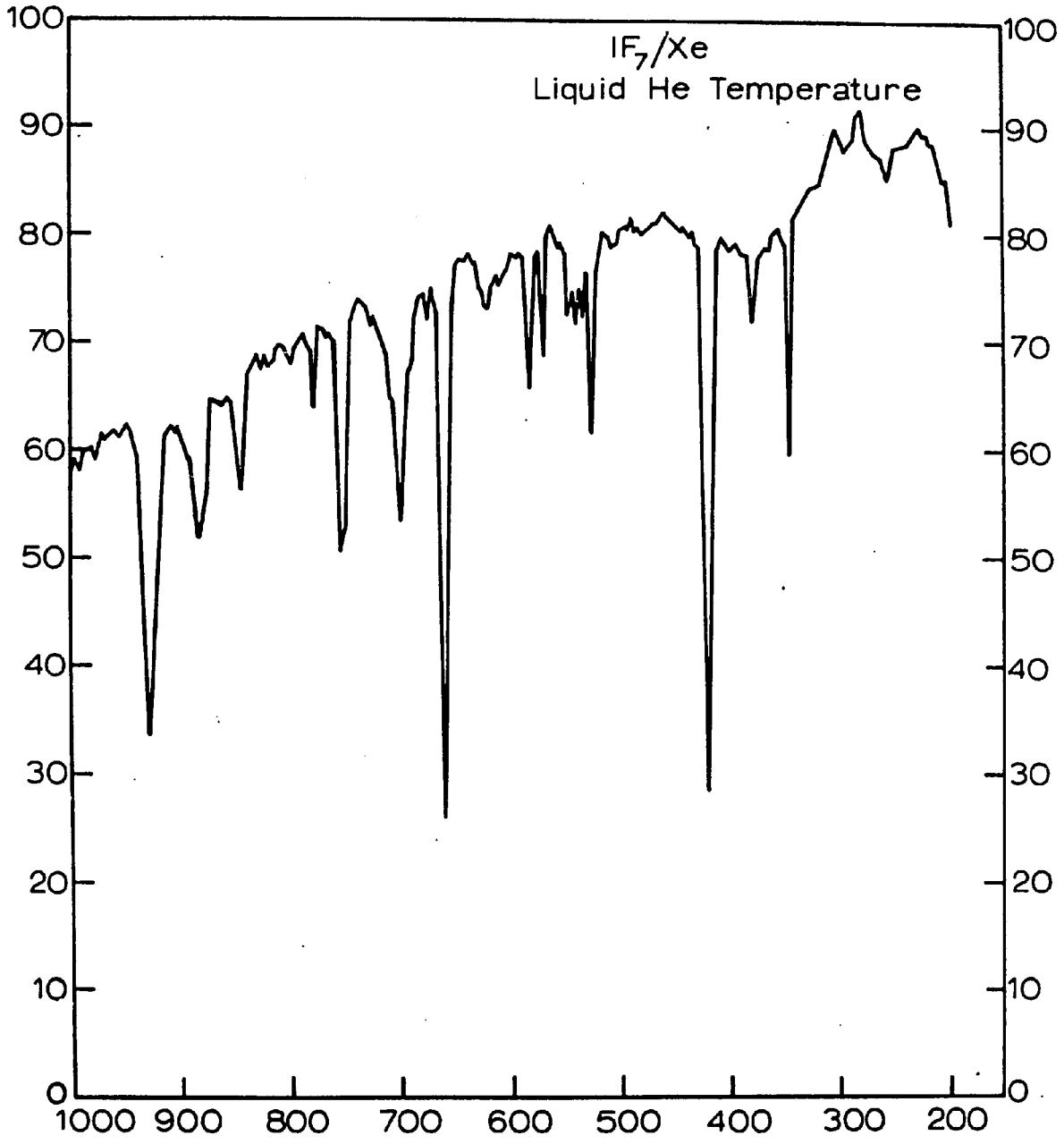

IF7/Xe
Liquid He Temperature
100
90
80
70
60
50
40
30
20
10
0
1000 900 800 700 600 500 400 300 200

Figure 2.7.

Table 2.6

IF_7/Xe Liquid Helium Temperature

Observed IR Absorptions[a]

257	IF_7
348	IOF_5
369	IF_7, IOF_5
421	IF_7
528	
536	
541	
549	(IOF_5)
571	(IOF_5)
583	IOF_5
621	IOF_5
661	IF_7
699	IOF_5
753	IF_7
779	IOF_5
844	IOF_5
882	IOF_5
927	IOF_5

[a] Frequencies in cm^{-1}.

of the IF_7 sample.

IF_7 in a Nitrogen Matrix

The spectrum of IF_7 isolated in a nitrogen matrix at liquid helium temperature appears in Figure 2.8. The frequencies have been tabulated and are presented in Table 2.7. A general observation of the spectrum shows a strong absorption near 927 cm^{-1}, indicating the presence of IOF_5. The actual peak is split with branches at 931 cm^{-1} and 938 cm^{-1}. Another strong absorption of IOF_5 is located near 700 cm^{-1} where the peak has also been split with branches at 695 cm^{-1} and 705 cm^{-1}. The relative intensities of the IF_7 absorptions compared to the IOF_5 absorptions are lower with much more IOF_5 in the matrix than IF_7. Only four of the IF_7 fundamentals are evident with the 257 cm^{-1} transition missing. The peaks of 526 cm^{-1}, 535 cm^{-1}, 541 cm^{-1}, and 549 cm^{-1} are in the spectrum. Four new absorptions were observed at 727 cm^{-1}, 803 cm^{-1}, 980 cm^{-1}, and 995 cm^{-1}. These frequencies have no counterparts in the gas phase IOF_5 spectrum although they could be IOF_5 transitions.

Solid IF_7 at Liquid Helium Temperature

The spectrum recorded for IF_7 condensed at liquid helium temperature is presented in Figure 2.9. The fre-

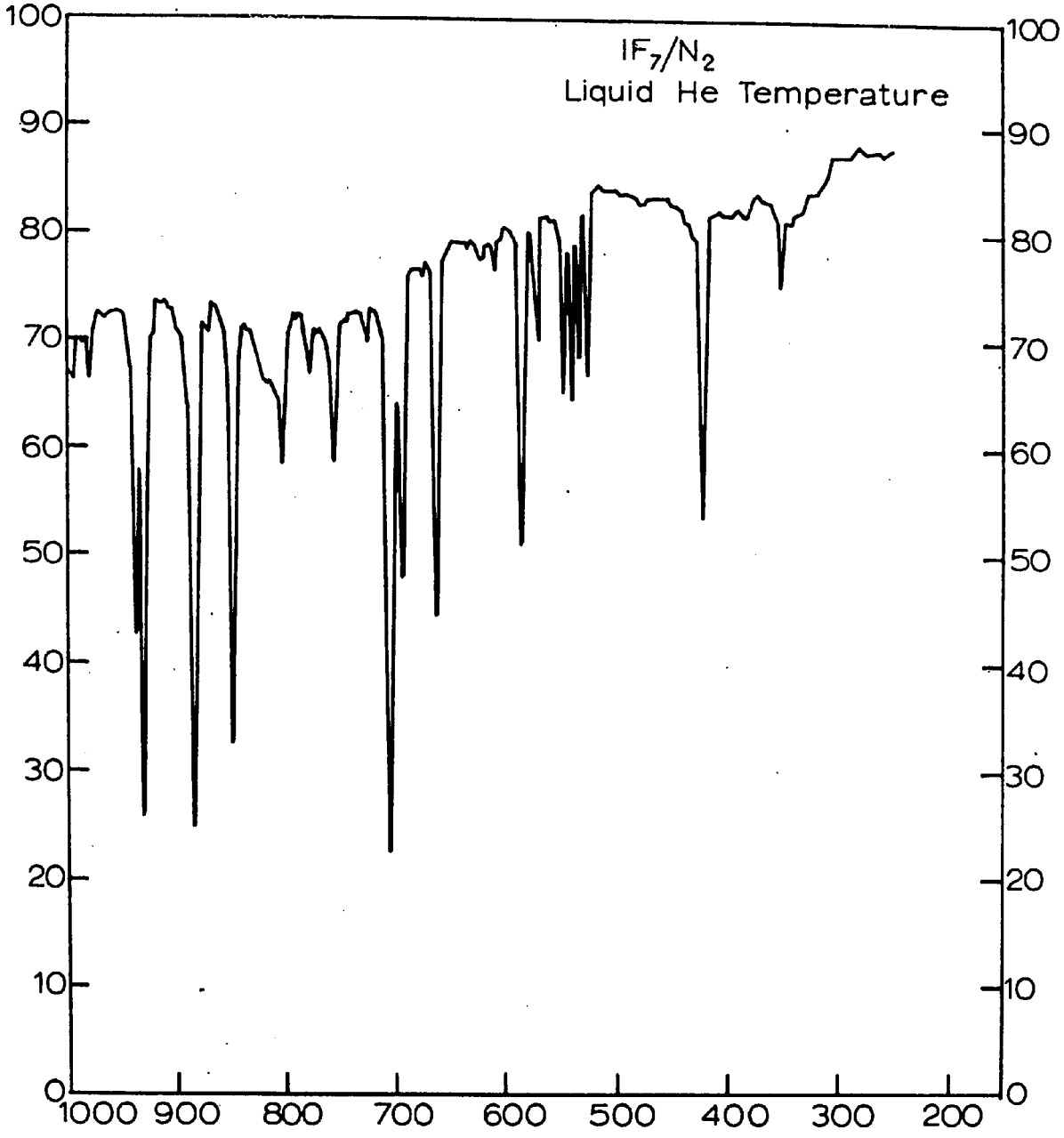

IF_7/N_2
Liquid He Temperature
100
90
80
70
60
50
40
30
20
10
0
1000 900 800 700 600 500 400 300 200

Figure 2.8.

Table 2.7

IF_7/N_2 Liquid Helium Temperature

Observed IR Frequencies[a]

351	IF_7
422	IF_7
526	
535	
541	
548	(IOF_5)[b]
571	(IOF_5)
586	IOF_5
610	IOF_5
662	IF_7
695	IOF_5
705	IOF_5
727	?
756	IF_7
779	IOF_5
803	?
849	IOF_5
884	IOF_5
931	IOF_5
938	IOF_5
980	?
995	?

[a] Frequencies in cm^{-1}.

[b] See text.

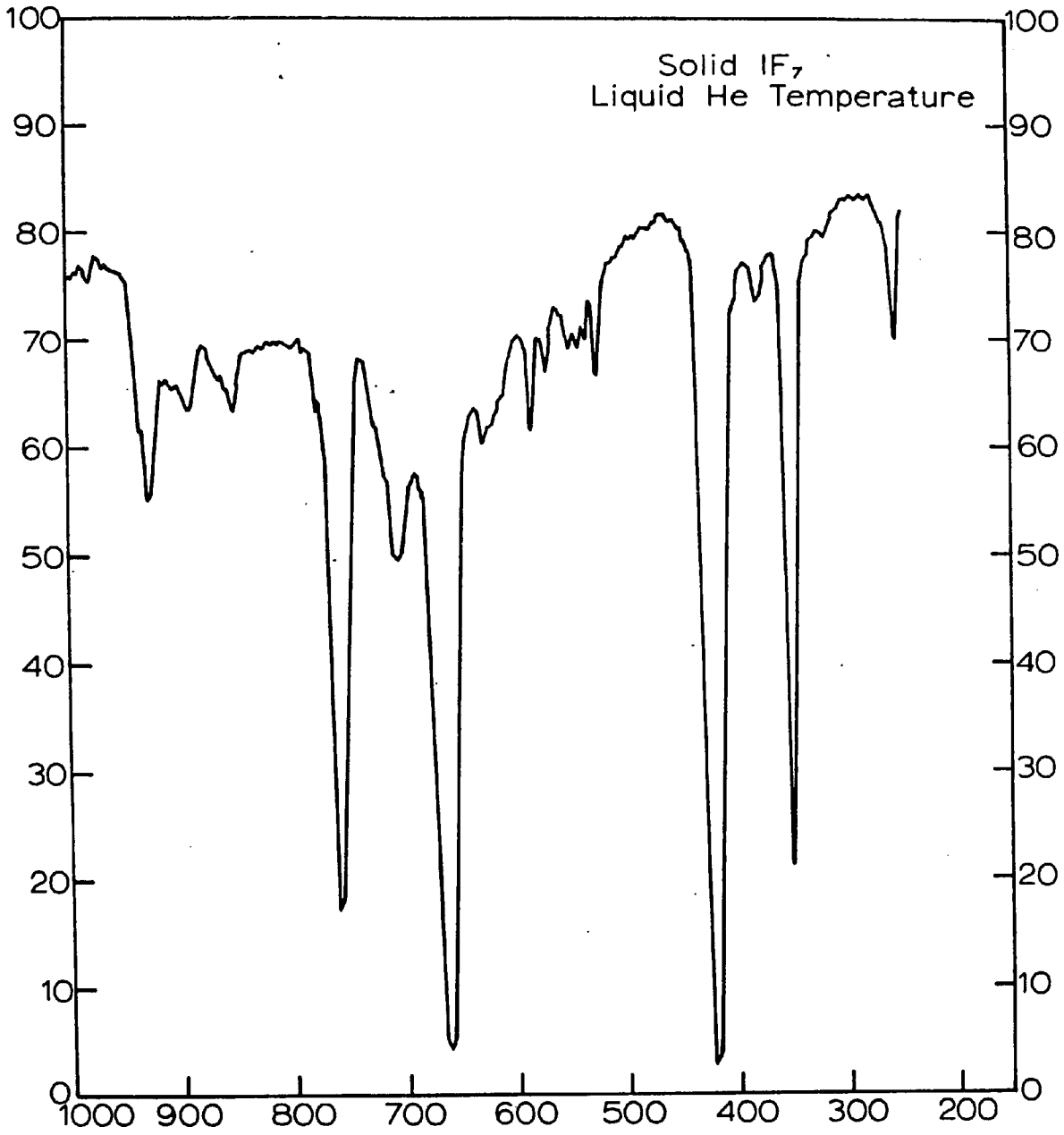

Solid IF_7
Liquid He Temperature
100
90
80
70
60
50
40
30
20
10
0
1000
900
800
700
600
500
400
300
200

Figure 2.9.

quencies are listed in Table 2.8. The five infrared fundamentals of IF_7 can be observed as well as the IOF_5 fundamentals. Absorptions corresponding to the IF_7 vibrations are strong and somewhat broader than a few of the other peaks on previous spectra. Vibrational frequencies for IOF_5 are less intense than the IF_7 frequencies but nonetheless IOF_5 is still present in the sample in significant quantities.

The frequencies which were reported for the IF_7 sample isolated in the other matrices are also present in this spectrum. Wherever the infrared absorptions can be assigned either to IF_7 or to IOF_5, the frequencies have been so marked in the tabulated list.

Not all the weak absorptions which appear in the spectrum were listed in Table 2.8 because there is already severe contamination of the IF_7 sample. There is also the possibility of other impurities besides the obvious IOF_5. In such a case it is difficult to accurately assign the frequencies, especially those belonging to the weak transitions in the spectrum.

Table 2.8

Solid IF_7 Liquid Helium Temperature

Observed Frequencies[a]	
257	IF_7
351	IF_7
370	IOF_5
421	IF_7
526	
537	
542	
550	(IOF_5)
571	(IOF_5)
585	IOF_5
630	IOF_5
663	IF_7
708	IOF_5
760	IF_7
779	IOF_5
852	IOF_5
892	IOF_5
928	IOF_5
980	?

[a] Frequencies in cm^{-1}.

DISCUSSION

Five spectra of iodine heptafluoride in the solid phase have been presented in the results section. Three of the spectra are matrix isolation spectra while the other two are solid IF_7. Both the solid IF_7 at liquid nitrogen temperature and the IF_7 in the argon matrix are free of impurities. On the other hand, the nitrogen and xenon matrices and the solid IF_7 sample at liquid helium temperature exhibited severe contamination. The spectra of the impure samples are reported for completeness although their reliability is not as great as the two pure samples.

Some of the weak absorptions due to the impurities were not assigned whereas all the peaks in the pure spectra were assigned as IF_7 vibrations. Wherever possible the impurity bands were assigned to IOF_5, which was the major and most obvious contaminant. IF_5 is a possible impurity from the IF_7 synthesis, but no peaks were attributed to the pentafluoride because the vibrational fundamental at 318 cm^{-1} was not observed in any of the spectra. Besides, the other IF_5 frequencies coincide with those of IF_7 or IOF_5.

The region of 250 cm^{-1} to 1000 cm^{-1} contains all the IF_7 fundamentals as well as those of IOF_5. The IF_7 combinations beyond 1000 cm^{-1} appear only at high concentrations and in fact were not observed in the two pure spectra. The other spectra are already complicated with the IOF_5

peaks and cannot add to the information available below 1000 cm^{-1}. All the reported spectra exhibit the IF_7 fundamentals except for the IF_7/Ar and IF_7/N_2 matrix spectra which do not show the weak 257 cm^{-1} band.

In the spectra containing large amounts of IOF_5 as evidenced by the 927 cm^{-1} absorption (Claassen's criterion for IF_7 purity) there are four transitions between 520 cm^{-1} and 550 cm^{-1} which are of uncertain origin. At the highest sample concentrations, Claassen reported unassigned peaks at 520 cm^{-1} and 837 cm^{-1} and attributed them to either combinations of the e_2'' vibration or complexes formed on the window. The 837 cm^{-1} peak was not observed although the spectra containing IOF_5 contamination showed a peak at 528 cm^{-1}. In the two spectra free of IOF_5 the 528 cm^{-1} band was not observed. So it is more likely that the 528 cm^{-1} absorption is an IOF_5 rather than a pseudo-rotation combination band. While two of these bands, 549 cm^{-1} and 571 cm^{-1}, are consistent with IOF_5 selection rules as binary combinations, the 528 cm^{-1} and 535 cm^{-1} bands remain unassigned. The 549 cm^{-1} and 571 cm^{-1} frequencies are tentatively assigned as new combination bands of IOF_5. The 779 cm^{-1} frequency which just appears in the gas phase IOF_5 spectrum can be assigned as a ternary combination.

Peak splitting of several IF_7 fundamentals was observed in the spectrum of solid IF_7 at liquid nitrogen temperature. Splitting was not observed in the IF_7 peaks of the other spectra. Two possible explanations are split-

tings due to differences in site symmetry or due to ligand field effects. The splittings were not observed in any other spectra. Consequently, since they were not reproduced, the splittings may not be real. Thus it is difficult to give an explanation for the observations in the liquid N_2 temperature spectrum.

In the solid IF_7 spectrum at liquid nitrogen temperature, the only features besides the fundamentals are background peaks (marked by dotted segments) and the bands on each side of the 665 cm^{-1} fundamental. These frequencies are 628 cm^{-1} and 710 cm^{-1}, respectively. Bernstein[8] and Khanna[19] have estimated the ν_{11} (e_2" frequency to be around 200 cm^{-1}. An $e_2" \times e_2'$ combination of $\nu_8 + \nu_{11}$ = 510 cm^{-1} + 200 cm^{-1} = 710 cm^{-1} is an infrared allowed band containing the a_2" species. Another combination, namely $e_2" \times e_2" \times e_2'$, with $2\nu_{11} + \nu_{10}$ would also lead to a 710 cm^{-1} combination.

As for the 628 cm^{-1} peak, a combination of $\nu_6 + \nu_{11}$ equals 625 cm^{-1}. The binary combination of $e_1' \times e_2"$ = $e_1" + e_2"$ is Raman but not infrared allowed. However, Durig and Wertz observed pseudorotational fine structure on the 1460 cm^{-1} band of cyclopentane.[10] Since the 1460 cm^{-1} vibration is an e_1' mode, the selection rules suggest an inactive combination. The pseudorotation model on the other hand is based on an anharmonic coupling of the $e_2"$ mode and the axial e_1' mode in the cubic term, $(e_2")^2$-

$(e_1')_{ax}$. In that case, the combination is indeed infrared allowed as seen with Durig's results on cyclopentane. It is therefore possible that the e_1' band at 425 cm^{-1} can combine with the pseudorotational frequency to produce an infrared active band.

The IF_7/Ar spectrum does not corroborate the above remarks because the 628 cm^{-1} and 710 cm^{-1} bands are not present. Iodine heptafluoride intensities are much lower for the argon matrix spectrum than for the solid IF_7 spectrum. So the weak bands may not be visible at the reduced concentrations. There is of course an intense IOF_5 peak at 710 cm^{-1} in the gas phase, and it could be argued that the 710 cm^{-1} absorption in the solid IF_7 spectrum is due to IOF_5 and not pseudorotation. Smith and Begun[18] claim the 710 cm^{-1} absorption is the most intense IOF_5 infrared band with the possibility that the 710 cm^{-1} peak would be visible while a less intense 927 cm^{-1} peak would not. However, in the solid phase spectra reported in this dissertation, the 710 cm^{-1} and 927 cm^{-1} gas phase absorptions are of comparable intensity. More importantly, the 710 cm^{-1} gas phase peak was shifted to lower frequencies (see tables) in each spectrum where IOF_5 was obviously present. It thus appears unlikely that the 710 cm^{-1} band in the solid IF_7 sample which shows no sign of a 927 cm^{-1} I = O stretching vibration is the e vibration of IOF_5.

CONCLUSION

This work was undertaken to search for pseudorotation in IF_7. Unequivocal proof for the validity of the pseudorotational model or hard and fast evidence of pseudorotation bands were not found. Nevertheless, conclusive proof that pseudorotation in IF_7 does not exist was not found either. On the contrary, the electron diffraction and molecular beam focusing experiments provide strong evidence in favor of a pseudorotational model which in the case of cyclopentane was demonstrated to be valid.

The difficulties encountered with a highly reactive molecule complicate the experimental problem of looking for pseudorotation bands which do not appear in the gas phase spectra. Pure samples of IF_7 can be obtained and can be examined in the solid phase or in inert matrices. Gas phase spectra lack the sharpness at high concentrations which are necessary to observe possible $e_2"$ bands which are expected to be weak.

Some new combination bands of IOF_5 have been proposed although an investigation of IOF_5 was not originally intended. Two possible pseudorotation bands were observed in the solid IF_7 sample at liquid nitrogen temperature. The new results uncovered in this investigation of IF_7 are encouraging and deserve continued effort to test the pseudorotational model.

REFERENCES

1. W. J. Adams, H. Bradford Thompson, and L. S. Bartell, J. Chem. Phys., 53, 4040 (1970).

2. L. S. Bartell in Physical Methods in Chemistry, 4th Edition, A. Weissberger and B. W. Rossiter, Eds., Interscience, New York, 1973.

3. John E. Kilpatrick, Kenneth S. Pitzer, and Ralph Spitzer, J. Amer. Chem. Soc., 69, 2483 (1947).

4. E. W. Kaiser, J. S. Muenter, W. Klemperer, and W. E. Falconer, J. Chem. Phys., 53, 53 (1970).

5. H. H. Claassen, E. L. Gasner, and H. Selig, J. Chem. Phys., 49, 1803 (1968).

6. R. C. Lord, M. A. Lynch, W. C. Schumb, and E. J. Slowinski, Jr., J. Amer. Chem. Soc., 72, 522 (1950).

7. Neil Bartlett and L. E. Levchuk, Proc. Chem. Soc., 1963, 342.

8. Lawrence S. Bernstein, Doctoral Dissertation, University of California, Berkeley, 1974.

9. E. Jean Jacob and L. S. Bartell, J. Chem. Phys., 53, 2235 (1970).

10. J. R. Durig and D. W. Wertz, J. Chem. Phys., 49, 2118 (1968).

11. N. Bartlett, S. Beaton, L. W. Reeves, and E. J. Wells, Can. J. Chem., 42, 2531 (1964).

12. Eric Whittle, David A. Dows, and George C. Pimentel, J. Chem. Phys., 22, 1943 (1954).

13. E. D. Becker and G. C. Pimentel, J. Chem. Phys., 25, 224 (1956).

14. See for example, A. L. Khidir Aljibury and R. L. Redington, J. Chem. Phys., 52, 453 (1970); R. A. Torey, R. L. Redington, and A. L. Khidir Aljiburg, J. Chem. Phys., 54, 344 (1971); S. T. King, J. Phys. Chem., 75, 405 (1971); H. H. Claassen and J. L. Huston, J. Chem. Phys., 55, 1505 (1971).

15. R. Caspary, Appl. Spectrosc., 22, 694 (1968).

16. G. Wilse Robinson, J. Molec. Spectr., 6, 58 (1961).

17. Gerhard Herzberg, Molecular Spectra and Molecular Structure, Vol. II, D. VanNostrand Company, Inc., New York, 1966.

18. D. F. Smith and G. M. Begun, J. Chem. Phys., 43, 2001 (1965).

19. R. K. Khanna, J. Molec. Spec., 8, 134 (1962).

PART III. THREE-ATOM SCATTERING.

In current gas phase electron diffraction theory the total diffraction intensity is the sum of atomic and molecular contributions.[1] The molecular intensities, based on scattering between nuclear pairs, contain the desired structural information. However, the Fourier sine transform of the reduced molecular intensity differs systematically from the functions calculated by the theory. The discrepancies increase with increasing atomic number as with ReF_6[2] where the structural analysis is significantly affected by heavy atom effects.

Bartell and Wong proposed a limiting case of corrections for the three-atom scattering[3] and later generalized their theory for polyatomic gas molecules.[4] In the limiting three-atom system, one atom may eclipse another for certain molecular orientations. The incident electrons scattered by the eclipsed atomic pair and the third atom undergo an attenuated diffraction.

Bartell and Wong have published a detailed account of the three-atom scattering theory[3,4] with derivations of the analytical three-atom equations[5] from a variant of the partial wave scattering theory. Fortran IV programs for the University of Michigan Terminal System were written or modified by C. L. Ritz.

In a three-atom scattering least squares of the intensities analysis, the three-atom contribution to the reduced

molecular intensity, M(s), is calculated and added to the two-atom M(s). The computations are performed by CLRLSI2, a modified version of the standard least squares program GCLSI (Geometrically Constrained Least Squares of the Intensities). The subroutine, CORINT (Corrected Intensities), calculates the three-atom intensities with the following equation:

$$I_{3atom} = \text{MULTIPLICITY} \times \frac{1}{Kr_{ij}^2} |f_i(s_i)||f_j(s_j)||f_k(s)| \times$$

$$\exp(-\ell_\perp^2 s^2/2) J_o\{s r_{jk} \sin\omega_{ijk}[1-\varepsilon(s)]\} \times$$

$$[\sin(\eta_i(s_i) + \eta_j(s_j) - \eta_k(s))]$$

and

$$\varepsilon(s) = \{\frac{1}{2r_{ij}^2} \frac{-f_i''(s_i)}{f_i(s_i)} - \frac{f_j''(s_j)}{f_j(s_j)} + \frac{2 f_i'(s_i) f_j'(s_j)}{f_i(s_i) f_j(s_j)}\}$$

In the above equations, i, j, and k, designate the three individual atoms in a particular three-atom combination where the multiplicity equals twice the occurrence of a given ijk set. The angle, <ijk, is designated as ω_{ijk}. The atomic elastic scattering factors are $f(s) = |f(s)| \times \exp[i\eta(s)]$ where $\eta(s)$ is the phase shift. The program CLRTABLE extrapolates tabulated f(s) values[6] and calculates f'(s) and f"(s) by a convolution method.[7] Only $f_k(s)$ is a true elastic scattering factor with $s = \frac{4\pi}{\lambda}\sin(\phi/2)$ whereas f_i and f_j are calculated from $s_i = [(r_{jk}/r_{ij})\cos\omega_{ijk}]\ s$ and $s_j = [1-(r_{jk}/r_{ij})\cos\omega_{ijk}]\ s$ where

r_{ij} and r_{jk} represent the distances between atoms i, j and j, k, respectively. In the current version of CLRLSI2, $l_{\perp}$, the perpendicular component of the amplitude of vibration, is calculated approximately.[8] The zeroth order Bessel function, J_o, is approximated with the following:

$$J_o(x) = (\cos x + \sin x)(\pi x)^{-1/2} \qquad (1)$$

The imaginary component of $\varepsilon(s)$ is small compared to the real part and is neglected in the calculations. CLRTABLE also calculates an appropriate three-atom background function for use in CLRLSI2.

Ritz successfully applied the three-atom scattering corrections to several molecules, most notably to ReF_6 and $XeOF_4$.[8] A preliminary examination of IF_7 revealed in the difference curve between the Fourier sine transforms of the theoretical and experimental reduced molecular intensity a pattern resembling that encountered in previous three-atom scattering corrections. The IF_7 diffraction data thus seemed susceptible to analysis and improvement by the three-atom treatment.

Adams' data extends from q = 16 $A^{\circ -1}$ to q = 163 $A^{\circ -1}$ ($q = \frac{10}{\pi}s$), but CLRLSI2 requires that q begin at -4 $A^{\circ -1}$ and terminate with a maximum of 145 $A^{\circ -1}$. An attempt to redimension the program without major changes was not successful. Consequently Adams' data were truncated at q = 140 $A^{\circ -1}$, and the new data set was subjected to the

standard least squares procedure. Since the CLRLSI2 results are based on a maximum q of 140 $A^{\circ -1}$ it was necessary to obtain geometric parameters, without three-atom corrections, based on a maximum q of 140 $A^{\circ -1}$. Since the three-atom corrections are small at large q, the removal of the last 23 intensity points has a minimal effect on the corrections.

Adams' molecular description for the C_2 conformation of IF_7 was chosen as a starting point. While the C_2 configuration has more three-atom combinations than the D_{5h} structure, the D_{5h} form has the intrinsic discrepancies associated with pseudorotation besides the three-atom scattering effects. The input description for IF_7, listed in Table 3.1, is in terms of an indexed system for internuclear distances, corresponding amplitudes of vibration, and atom numbers. The atomic numbering scheme for ijk sets is as follows. Atom 2 is the iodine atom, 8 and 9 are the axial fluorines, atoms 3 through 7 are the equatorial fluorines in clockwise arrangement, and atom 1 is a dummy superimposed on atom 8 in the D_{5h} reference. Adams' C_2 molecular description includes 23 internuclear distances (not all distinct), 9 atoms, and 4 amplitudes of vibration.

Ritz reported a significant decrease in the estimated standard deviations of the composite molecular intensities for both ReF_6 and $XeOF_4$. The standard deviation for the C_2 conformation of IF_7 obtained by the conventional least

Table 3.1

IF_7 3 Atom Input									C_2 Conformation
r_{ij}	r_{jk}	r_{ik}	i	j	k	l_i	l_j	l_k	Multiplicity
1	1	3	4	2	3	1	1	2	8
1	1	5	5	2	4	1	1	2	8
1	1	6	6	2	5	1	1	2	4
1	1	19	5	2	3	1	1	4	8
1	1	21	6	2	4	1	1	4	8
1	1	22	4	2	7	1	1	4	4
2	8	1	2	8	3	1	3	1	4
2	10	1	2	8	4	1	3	1	4
2	12	1	2	8	5	1	3	1	4
2	14	1	2	8	6	1	3	1	4
2	16	1	2	8	7	1	3	1	4
22	4	3	4	7	3	4	2	2	2
19	3	5	5	3	4	4	2	2	4
21	5	6	6	4	5	4	2	2	4
21	20	3	4	6	3	4	4	2	8
23	22	5	5	7	4	4	4	2	8
20	19	6	6	3	5	4	4	2	4
5	19	3	4	5	3	2	4	2	8
6	21	5	5	6	4	2	4	2	8
22	4	3	4	7	3	4	2	2	4
6	20	19	5	6	3	2	4	4	4
7	22	21	6	7	4	2	4	4	8
4	19	23	7	3	5	2	4	4	8
10	8	3	4	8	3	3	3	2	8
12	10	5	5	8	4	3	3	2	8
14	12	6	6	8	5	3	3	2	8
16	14	7	7	8	6	3	3	2	8
8	16	4	3	8	7	3	3	2	8
12	8	19	5	8	3	3	3	4	8
14	10	21	6	8	4	3	3	4	8

Table 3.1 continued.

r_{ij}	r_{jk}	r_{ik}	i	j	k	l_i	l_j	l_k	Multiplicity
16	12	23	7	8	5	3	3	4	8
14	8	20	6	8	3	3	3	4	8
16	10	22	7	8	4	3	3	4	8
18	8	9	9	8	3	4	3	3	2
18	10	11	9	8	4	4	3	3	4
18	12	13	9	8	5	4	3	3	4
3	1	1	3	4	2	2	1	1	8
5	1	1	4	5	2	2	1	1	4
19	1	1	3	5	2	4	1	1	8
21	1	1	4	6	2	4	1	1	8
22	1	1	7	4	2	4	1	1	4
8	2	1	3	8	2	3	1	1	4
10	2	1	4	8	2	3	1	1	4
12	2	1	5	8	2	3	1	1	4
14	2	1	6	8	2	3	1	1	4
16	2	1	7	8	2	3	1	1	4
1	2	8	3	2	8	1	1	3	4
1	2	10	4	2	8	1	1	3	4
1	2	12	5	2	8	1	1	3	4
1	2	14	6	2	8	1	1	3	4
1	2	16	7	2	8	1	1	3	4
3	10	8	3	4	8	2	3	3	4
5	12	10	4	5	8	2	3	3	4
6	14	12	5	6	8	2	3	3	4
7	16	14	6	7	8	2	3	3	4
4	8	16	7	3	8	2	3	3	4
19	12	8	3	5	8	4	3	3	4
21	14	10	4	6	8	4	3	3	4
20	8	14	6	3	8	4	3	3	4
22	16	10	4	7	8	4	3	3	4
23	16	12	5	7	8	4	3	3	4
9	18	8	3	9	8	3	4	3	4

Table 3.1 continued.

r_{ij}	r_{jk}	r_{ik}	i	j	k	l_i	l_j	l_k	Multiplicity
11	18	10	4	9	8	3	4	3	4
13	18	12	5	9	8	3	4	3	4
15	18	14	6	9	8	3	4	3	4
17	18	16	7	9	8	3	4	3	4

squares procedure without three-atom refinement on 125 intensity points is 0.0014. However, the standard deviation on the C_2 conformer with three-atom refinement is 0.0019, which is a significant increase over 0.0014.

The program input was checked for errors which might produce an increased standard deviation. Several minor errors were uncovered but with no subsequent change in the standard deviation. The next step was a thorough investigation of the three-atom program itself. No errors in the main program or in the subroutines were detected. The mathematical approximation methods were also checked and found to be valid. The alternative was that the three-atom theory produced the increase in the standard deviations.

The three-atom scattering contribution denoted by $M(q)_{3atom}$ is added to the theoretical reduced molecular intensity, $M(q)_{TH}$, and the sum subtracted from the experimental intensity, $M(q)_{EXP}$,

$$M(q)_{EXP} - [M(q)_{TH} + M(q)_{3atom}] = \Delta M(q) - M(q)_{3atom} \quad (2)$$

where $\Delta M(q)$ represents the residual without the three-atom correction.

To best see the results for IF_7 the three-atom corrections are plotted against their corresponding q points in Figure 3.1. Along with the corrections are the residuals without three-atom refinement and the residuals of IF_7

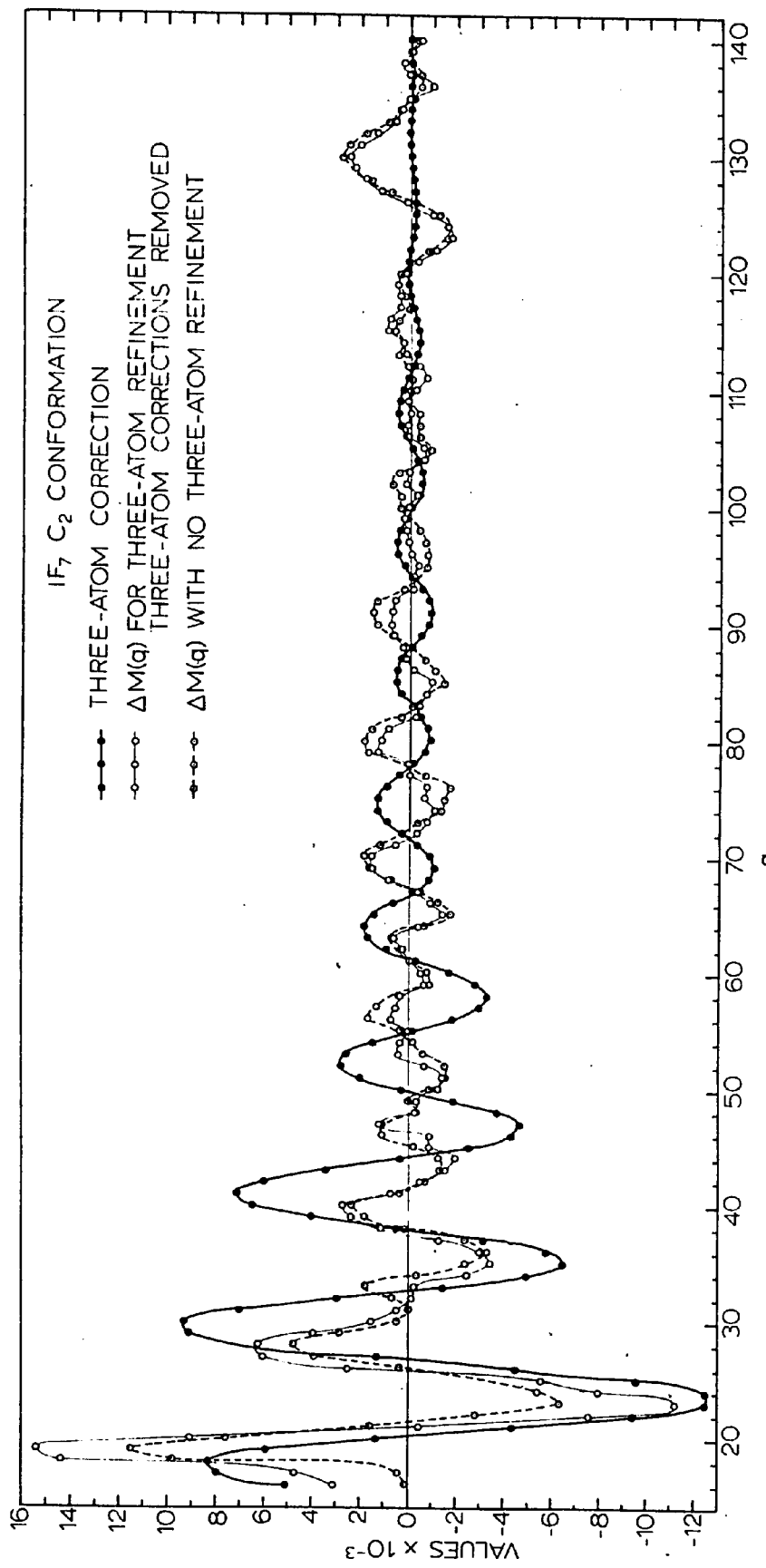


Figure 3.1. Three-atom Corrections and Residuals from Least Squares of the Intensities Refinement.

refined by the three-atom procedure but with the corrections removed. The graph shows that the corrections are large at small q but damp out to small values as q increases. The residuals with and without the three-atom refinement are practically in phase throughout the entire q range. The high bump in the residuals around q = 130 $A^{\circ -1}$ is possibly due to a minor defect in the experimental data.

Most noteworthy is the fact that at small q, below q = 40 $A^{\circ -1}$, the corrections and the residuals are nearly in phase. Between q = 40 $A^{\circ -1}$ and q = 50 $A^{\circ -1}$, however, the corrections move out of phase with the residuals to the extent that beyond q = 55 the corrections are essentially 180 degrees out of phase. From Equation (2) it can be seen that the three-atom corrections increase the value of the residuals when the corrections and residuals are out of phase and to the greatest amount when they are 180 degrees out of phase. The net result is that the three-atom refinement in the case of IF_7 has increased the discrepancies between theory and experiment.

As a further test of the three-atom scattering theory, ReF_7 was investigated. For sake of comparison with IF_7, the C_2 conformation of ReF_7 was selected, and the diffraction data of Jacob[9] were subjected to the least squares procedure. ReF_7 was described in terms of 23 internuclear distances, 9 atoms, and 4 amplitudes of vibration so that the program input would be similar to that for IF_7 with

only the parameter values changed.

Jacob and Bartell refined ReF_7 with a crude "heavy atom" correction based on an analysis of ReF_6, and reported the structure with a standard deviation of the molecular intensities equal to 0.0011. The refinement of the ReF_7 intensities with three-atom corrections led to a standard deviation of 0.0018, a significant increase over that of the previous analysis.

The three-atom corrections for ReF_7 and the residuals for the three-atom refinement with the three-atom corrections removed are presented in Figure 3.2. Like the corrections for IF_7, the corrections for ReF_7 are large at small q and decrease with increasing q values. A bump in the residuals occurs at the end of the data set around q = 120 $A^{\circ -1}$. The graph shows that the corrections and the residuals are of comparable magnitude up to q = 110 $A^{\circ -1}$ and are much closer in phase than the corresponding IF_7 curves. Up to q = 50 $A^{\circ -1}$ and beyond q = 60 $A^{\circ -1}$ the curves are only slightly out of phase but almost coincident between q = 50 $A^{\circ -1}$ and q = 60 $A^{\circ -1}$. The corrections and residuals, however, are sufficiently out of phase to produce a significant increase in the standard deviation of the composite molecular intensity.

PARAMETER ALTERATIONS

The three-atom corrections are made in conjunction with a least squares analysis of the diffraction intensi-

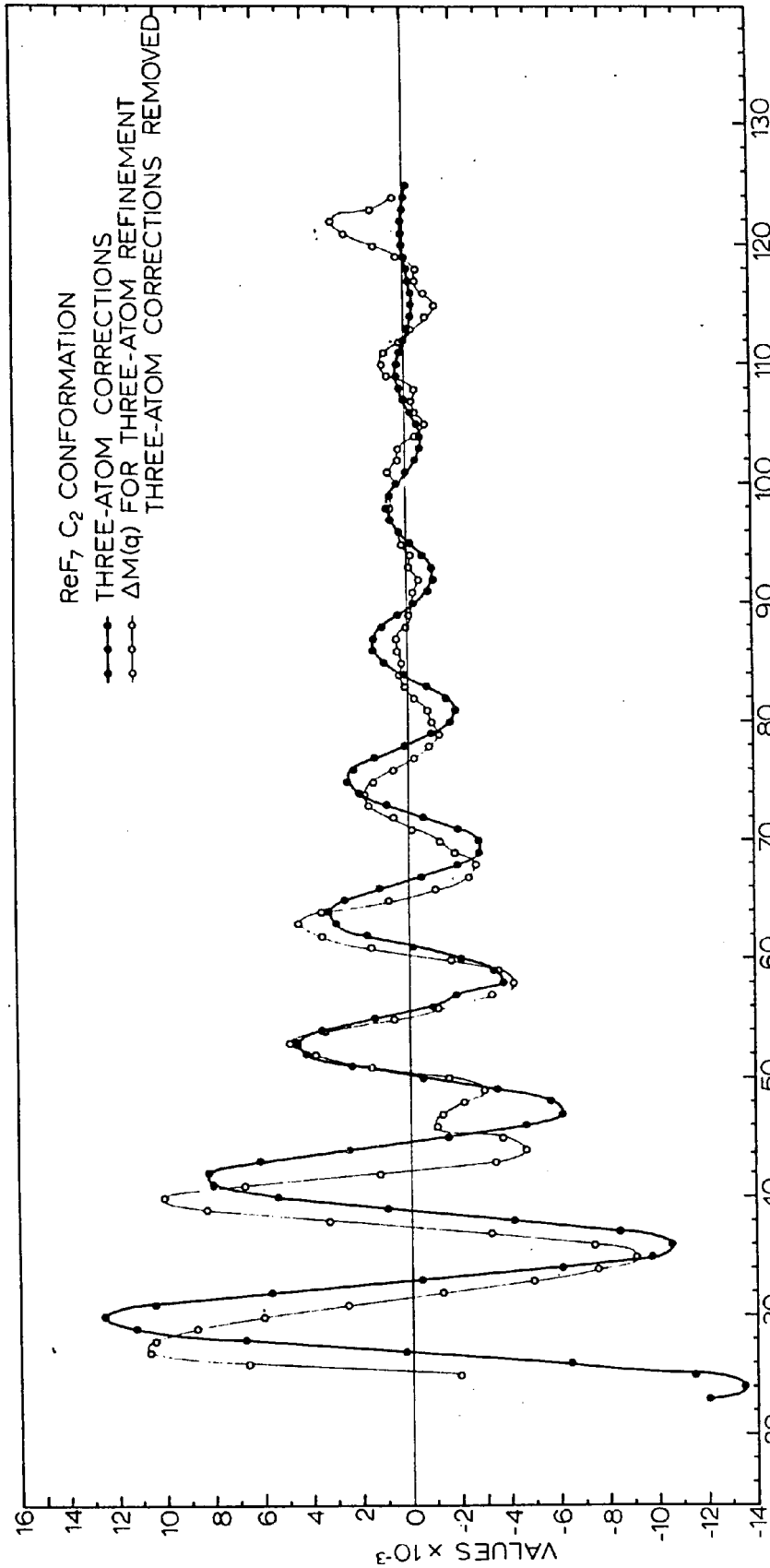


Figure 3.2. Three-atom Corrections and Residuals from Least Squares of the Intensities Refinement.

ties. So it is not surprising that the values of the geometric parameters change with the three-atom refinement. Table 3.2 and Table 3.3 list the parameters for the C_2 conformations of IF_7 and ReF_7, respectively. In column 1 of Table 3.2 the original refinement of 148 intensity points of IF_7 is reported. The remaining columns are the refinements of 125 points with and without the three-atom corrections.

The greatest change occurs in the standard deviation of the intensities where the three-atom refinement increased the error by 36% from 1.4 ppt to 1.9 ppt. The differences between the parameters of the two least squares analyses are within the limits of the estimated errors. However, the tabulated values indicate the trend of the parameter shifts.

The results on the C_2 conformation of ReF_7 are presented in Table 3.3 with the published parameters of Jacob and Bartell[9] in column 1. Column 3 lists the parameters obtained by Ritz with 6 three-atom combinations, based on the D_{5h} reference but applied to an actual C_2 geometry, while column 2 contains the parameters for 67 three-atom combinations. The sums of the multiplicities for 6 and 67 combinations, respectively, are the same. Like the estimated error for IF_7, the standard deviation of the intensities for ReF_7 is markedly higher for the three-atom refinement than for the refinement without the corrections. However, a significant improvement in the rhenium-fluorine

Table 3.2

IF_7 C_2 Conformation: Parameters[a] and Estimated Uncertainties[b]

	Original Results	No three-atom refinement	Three-atom refinement
Mean Bond	1.837	1.837 ± 0.02	1.842 ± 0.004
Axial-Equatorial Difference	0.072	0.070 ± 0.006	0.064 ± 0.008
Equatorial Pucker Angle	7.61	7.42 ± 1.06	7.10 ± 0.52
Axial Bend Angle	4.49	3.68 ± 1.18	4.65 ± 0.54
I-F Amplitude	0.045	0.040 ± 0.002	0.045 ± 0.002
Short F-F Amplitude	0.061	0.063 ± 0.007	0.062 ± 0.009
Axial-Equatorial F-F Amplitude	0.104	0.100 ± 0.010	0.103 ± 0.016
Long F-F Amplitude	0.091	0.082 ± 0.010	0.089 ± 0.014
R_f Index of Resolution	1.00	0.96 ± 0.02	0.99 ± 0.04
$\sigma(I)/\langle I\rangle$	1.345 PPT	1.4 PPT	1.9 PPT
q max	163	140	140

[a] Distance and amplitudes in Å, angles in degrees.

[b] Estimated uncertainties include the effects of both systematic and random errors reported as 2σ.

Table 3.3

ReF_7 C_2 Conformation: Parameters[a] and Estimated Uncertainties[b]

	Original Results	Three-Atom Refinement	
		67 Combinations	6 Combinations
Mean Bond	1.835 ± 0.005	1.841 ± 0.006	1.841
Axial-Equatorial Difference	0.065[c]	0.057 ± 0.016	0.048
Ring Pucker	8.78 ± 3.0	9.47 ± 1.0	9.62
Axial Bend	7.65 ± 3.0	9.27 ± 1.4	8.74
Re-F Amplitude	0.032 ± 0.004	0.041 ± 0.015	0.037[c] (± 0.010)[d]
Short F-F Amplitude	0.100[c]	0.075 ± 0.020	0.088[c]
Axial-Equatorial F-F Amplitude	0.103[c]	0.086 ± 0.032	0.085[c]
Long F-F Amplitude	0.125 ± 0.011	0.132 ± 0.036	0.120[c]
R	0.973	1.04	1.01
$\sigma(I)/\langle I\rangle$	1.08 PPT	1.75 PPT	1.67 PPT

[a] Distances and amplitudes in Å, angles in degrees.

[b] Estimated uncertainties include the effects of both systematic and random errors reported as 2σ.

[c] Not varied in final refinement.

[d] Error estimate from nonrefined structure.

bonded amplitude was made. The l_g(Re-F) in ReF_6 has a value of 0.044 A° ± 0.010 A° which is in excellent agreement with other 5d transition metal hexafluoride amplitudes.[2] The l_g(Re-F) previously reported for ReF_7 was 0.032 A° ± 0.004 A°. The three-atom refinement (6 combinations) gave a value of 0.037 A° ± 0.010 A° whereas the refinement with 67 combinations resulted in an l_g(Re-F) value of 0.041 A° ± 0.006 A° which agrees with 0.044 A° ± 0.010 A° from the ReF_6 structure. The other amplitudes are the same within the estimated errors.

CONCLUSIONS

The three-atom theory failed to lower the standard deviation of the reduced molecular intensity. On the one hand, the theory seems to work for molecules with 90° (and of course 180°) bond angles while on the other hand, it seems to fail when nonperpendicular bond angles are encountered. However, the four molecules* tested hardly represent a sufficient sample to prove or disprove the three-atom theory. At this time all that can be said is that the theory does not work for IF_7 or for ReF_7. The phase discrepancies between the corrections and residuals suggest that phase effects in the argument of J_o might offset the corrections to increase the standard error.

---

* Ritz obtained a modest improvement on $Pt[P(CH_3)_4]_4$.

The principles behind the three-atom theory appear to be sound even though the theory itself needs further examination with possible changes. Obviously more molecules should be investigated in an attempt to locate the exact shortcomings of the theory. A completely new computer program is highly recommended to replace CLRLSI2 which, as stated before, is only a modified version of the standard least squares program. A new three-atom program would probably require the services of an experienced programmer but would be much more efficient. Furthermore, the limitations and possible undetected errors in CLRLSI2 could then be eliminated.

REFERENCES

1. L. S. Bartell in Physical Methods in Chemistry, 4th Edition, A. Weissberger and B. W. Rossiter, Eds., Interscience Publishers, New York, 1973.

2. E. Jean Jacob and L. S. Bartell, J. Chem. Phys., 53, 2231 (1970).

3. L. S. Bartell and T. C. Wong, J. Chem. Phys., 56, 2364 (1971).

4. T. C. Wong and L. S. Bartell, J. Chem. Phys., 58, 5654 (1973).

5. Numerical methods have been proposed. See, for example, J. A. Hoerni, Phys. Rev., 102, 1530 (1956); P. J. Bunyan, Proc. Roy. Soc. (London), 82, 1051 (1963); J. Ginnes, Acta Cryst., 13, 1075 (1964); R. A. Bonham, J. Chem. Phys., 43, 1103 (1965); Trans. Am. Cryst. Assoc., 2, 165 (1966).

6. L. Schafer, A. C. Yates, and R. A. Bonham, J. Chem. Phys., 55, 3055 (1971).

7. A. Ravitzky and M. J. E. Goly, Anal. Chem., 36, 1627 (1964).

8. C. L. Ritz, Doctoral Dissertation, University of Michigan, 1974.

9. E. Jean Jacob and L. S. Bartell, J. Chem. Phys., 53, 2235 (1970).

APPENDICES

Appendix A: Experimental Leveled Intensity and Background Intensity Functions for $[(CH_3)_3Si]_3SiH$.

21 cm Camera Distance (r^3 sector)

s	$I_o(s)$	$I_B(s)$
3.132	2.4407	2.6639
3.252	2.6325	2.7072
3.373	2.7961	2.7456
3.493	2.9163	2.7793
3.613	2.9781	2.8089
3.733	3.0248	2.8347
3.854	3.0227	2.8573
3.974	2.9984	2.8770
4.094	2.9624	2.8940
4.215	2.9400	2.9087
4.335	2.8958	2.9214
4.455	2.9205	2.9322
4.575	2.9185	2.9414
4.695	2.8984	2.9491
4.816	2.8574	2.9556
4.936	2.8031	2.9609
5.056	2.7584	2.9652
5.176	2.7305	2.9687
5.296	2.7181	2.9714
5.416	2.7286	2.9734
5.537	2.7718	2.9748
5.657	2.8266	2.9757
5.777	2.8830	2.9762
5.897	2.9262	2.9763
6.017	2.9537	2.9760
6.137	2.9721	2.9755
6.257	2.9777	2.9747
6.377	2.9851	2.9738
6.497	2.9878	2.9726
6.617	2.9980	2.9713
6.737	3.0106	2.9699
6.857	3.0286	2.9684
6.976	3.0510	2.9669
7.096	3.0750	2.9653
7.216	3.0963	2.9636
7.336	3.1137	2.9619
7.456	3.1218	2.9602
7.576	3.1283	2.9586
7.695	3.1320	2.9569
7.815	3.1415	2.9552
7.935	3.1526	2.9536
8.054	3.1607	2.9520
8.174	3.1550	2.9504
8.294	3.1337	2.9489
8.413	3.0943	2.9474
8.533	3.0392	2.9459
8.652	2.9745	2.9445
8.772	2.9097	2.9432
8.892	2.8528	2.9418
9.011	2.8094	2.9406
9.131	2.7754	2.9394
9.250	2.7518	2.9382
9.369	2.7355	2.9371
9.489	2.7286	2.9360
9.608	2.7266	2.9350
9.727	2.7347	2.9340
9.847	2.7489	2.9328
9.966	2.7755	2.9317
10.085	2.8126	2.9308
10.204	2.8544	2.9302
10.324	2.8987	2.9296
10.443	2.9460	2.9290
10.562	2.9888	2.9283
10.681	3.0226	2.9276
10.800	3.0504	2.9270
10.919	3.0722	2.9264
11.038	3.0824	2.9259
11.157	3.0847	2.9254
11.276	3.0774	2.9249
11.395	3.0572	2.9244
11.514	3.0258	2.9240
11.632	2.9896	2.9236
11.751	2.9471	2.9232
11.870	2.9006	2.9228
11.989	2.8577	2.9225
12.107	2.8258	2.9222
12.226	2.8041	2.9219
12.345	2.7971	2.9216
12.463	2.7984	2.9214
12.582	2.8150	2.9211
12.700	2.8362	2.9209
12.819	2.8636	2.9207
12.937	2.8882	2.9206
13.056	2.9135	2.9204
13.174	2.9321	2.9202
13.292	2.9512	2.9201
13.411	2.9670	2.9200
13.529	2.9792	2.9199
13.647	2.9907	2.9198
13.765	2.9995	2.9198
13.883	3.0064	2.9197
14.001	3.0101	2.9197
14.119	3.0092	2.9197
14.237	3.0076	2.9197
14.355	2.9988	2.9197
14.473	2.9850	2.9197
14.591	2.9693	2.9198
14.709	2.9507	2.9198
14.827	2.9306	2.9199
14.944	2.9078	2.9200
15.062	2.8812	2.9202
15.180	2.8581	2.9203
15.297	2.8398	2.9205
15.415	2.8217	2.9207
15.533	2.8149	2.9209
15.650	2.8133	2.9212
15.767	2.8194	2.9215
15.885	2.8282	2.9218
16.002	2.8437	2.9221
16.120	2.8653	2.9225
16.237	2.8875	2.9229
16.354	2.9083	2.9233
16.471	2.9284	2.9238
16.588	2.9434	2.9243
16.705	2.9582	2.9249
16.822	2.9699	2.9255
16.939	2.9786	2.9262
17.056	2.9846	2.9269
17.173	2.9867	2.9276
17.290	2.9848	2.9284
17.407	2.9812	2.9293
17.523	2.9756	2.9302
17.640	2.9684	2.9311
17.757	2.9639	2.9322
17.873	2.9567	2.9333
17.990	2.9498	2.9344
18.106	2.9427	2.9357
18.223	2.9406	2.9370
18.339	2.9361	2.9383
18.455	2.9341	2.9398
18.572	2.9325	2.9413
18.688	2.9298	2.9430
18.804	2.9290	2.9447
18.920	2.9298	2.9465
19.036	2.9318	2.9484
19.152	2.9331	2.9504
19.268	2.9344	2.9525
19.384	2.9383	2.9547
19.500	2.9431	2.9570
19.616	2.9503	2.9595
19.731	2.9536	2.9620
19.847	2.9608	2.9647
19.963	2.9682	2.9675
20.078	2.9726	2.9704
20.194	2.9737	2.9734
20.309	2.9802	2.9766
20.425	2.9839	2.9867
20.540	2.9901	3.1462
20.655	2.9973	3.1520
20.770	3.0021	
20.886	3.0049	

11 cm Camera Distance (r^3 sector)

s	$I_o(s)$	$I_B(s)$
8.806	5.4408	
9.049	5.2480	
9.292	5.1623	
9.535	5.1382	
9.778	5.1581	
10.020	5.2797	
10.263	5.4413	
10.506	5.6243	
10.748	5.7829	
10.990	5.8582	5.5442
11.232	5.8458	5.5397
11.474	5.7609	5.5353
11.716	5.6066	5.5308
11.958	5.4188	5.5263
12.199	5.2961	5.5217
12.441	5.2777	5.5171
12.682	5.3333	5.5124
12.923	5.4424	5.5077
13.164	5.5381	5.5029
13.405	5.6037	5.4980
13.646	5.6541	5.4932
13.886	5.6687	5.4883
14.126	5.6693	5.4834
14.366	5.6376	5.4786
14.606	5.5690	5.4737
14.846	5.4795	5.4689
15.086	5.3747	5.4641
15.325	5.2796	5.4592
15.564	5.2298	5.4544
15.803	5.2343	5.4496
16.042	5.2887	5.4449
16.281	5.3685	5.4401
16.519	5.4454	5.4354
16.758	5.4967	5.4307
16.996	5.5295	5.4259
17.234	5.5337	5.4212
17.471	5.5152	5.4165
17.709	5.4815	5.4117
17.946	5.4391	5.4070
18.183	5.4115	5.4022
18.420	5.3864	5.3975
18.657	5.3673	5.3927
18.893	5.3539	5.3881
19.129	5.3486	5.3834
19.365	5.3485	5.3788
19.601	5.3600	5.3742
19.836	5.3641	5.3697
20.072	5.3701	5.3651
20.307	5.3713	5.3606
20.542	5.3737	5.3561
20.776	5.3788	5.3515
21.011	5.3764	5.3470
21.245	5.3723	5.3424
21.479	5.3546	5.3378
21.712	5.3393	5.3333
21.945	5.3179	5.3287
22.179	5.2937	5.3242
22.411	5.2768	5.3196
22.644	5.2609	5.3151
22.876	5.2585	5.3106
23.108	5.2646	5.3061
23.340	5.2801	5.3017
23.572	5.3034	5.2973
23.803	5.3230	5.2931
24.034	5.3425	5.2889
24.265	5.3471	5.2848
24.495	5.3394	5.2807
24.726	5.3259	5.2768
24.955	5.3026	5.2730
25.185	5.2694	5.2693
25.414	5.2411	5.2657
25.644	5.2204	5.2622
25.872	5.2033	5.2588
26.101	5.2031	5.2556
26.329	5.2070	5.2525
26.557	5.2250	5.2495
26.785	5.2453	5.2467
27.012	5.2625	5.2440
27.239	5.2759	5.2415
27.466	5.2800	5.2391
27.692	5.2747	5.2369
27.918	5.2629	5.2348
28.144	5.2441	5.2328
28.370	5.2264	5.2310
28.595	5.2149	5.2293
28.820	5.2010	5.2277
29.044	5.1966	5.2263
29.269	5.1997	5.2250
29.493	5.2070	5.2238
29.716	5.2203	5.2228
29.940	5.2298	5.2219
30.163	5.2404	5.2212
30.385	5.2424	5.2207
30.608	5.2441	5.2203
30.830	5.2423	5.2200
31.051	5.2348	5.2198
31.273	5.2316	5.2198
31.494	5.2238	5.2199
31.715	5.2197	5.2201
31.935	5.2162	5.2204
32.155	5.2121	5.2208
32.375	5.2133	5.2214
32.594	5.2116	5.2220
32.813	5.2138	5.2228
33.032	5.2190	5.2238
33.250	5.2241	5.2249
33.468	5.2277	5.2261
33.686	5.2319	5.2275
33.903	5.2386	5.2290
34.120	5.2413	5.2306
34.337	5.2408	5.2323
34.553	5.2441	5.2341
34.769	5.2432	5.2361
34.985	5.2422	5.2382
35.200	5.2398	5.2403
35.415	5.2418	5.2426
35.629	5.2419	5.2449
35.843	5.2390	5.2474
36.057	5.2436	5.2500
36.271	5.2463	5.2526
36.484	5.2491	5.2551
36.697	5.2557	5.2578
36.909	5.2601	5.2605
37.121	5.2660	5.2634
37.332	5.2724	5.2665
37.544	5.2757	5.2698
37.755	5.2825	5.2734
37.965	5.2791	5.2772
38.175	5.2822	5.2813
38.385	5.2838	5.2857
38.595	5.2835	5.2904
38.804	5.2868	5.2955
39.012	5.2941	5.3009
39.221	5.3007	5.3067
39.428	5.3065	5.3129
39.636	5.3201	5.3196
39.843	5.3245	5.3267
40.050	5.3320	5.6648
40.256	5.3391	
40.462	5.3484	
40.668	5.3521	

21 cm Camera Distance (r^2 sector)

s	$I_o(s)$	$I_B(s)$
2.091	1.1643	1.0656
2.152	1.1417	1.0771
2.214	1.1132	1.0886
2.275	1.1089	1.1000
2.337	1.0987	1.1113
2.398	1.0862	1.1225
2.459	1.0730	1.1336
2.521	1.0585	1.1447
2.582	1.0465	1.1556
2.644	1.0397	1.1664
2.705	1.0378	1.1772
2.767	1.0376	1.1878
2.828	1.0435	1.1983
2.889	1.0562	1.2088
2.951	1.0728	1.2191
3.012	1.0965	1.2293
3.074	1.1239	1.2394
3.135	1.1527	1.2495
3.197	1.1811	1.2594
3.258	1.2136	1.2691
3.319	1.2459	1.2788
3.381	1.2733	1.2884
3.442	1.2967	1.2978
3.504	1.3186	1.3071
3.565	1.3388	1.3163
3.626	1.3549	1.3254
3.688	1.3709	1.3344
3.749	1.3824	1.3432
3.811	1.3915	1.3520
3.872	1.4007	1.3606
3.933	1.4095	1.3690
3.995	1.4145	1.3774
4.056	1.4184	1.3856
4.117	1.4245	1.3937
4.179	1.4286	1.4017
4.240	1.4350	1.4096
4.302	1.4406	1.4173
4.363	1.4473	1.4249
4.424	1.4546	1.4323
4.486	1.4593	1.4397
4.547	1.4630	1.4469
4.608	1.4656	1.4540
4.670	1.4665	1.4609
4.731	1.4657	1.4678
4.792	1.4617	1.4745
4.854	1.4578	1.4810
4.915	1.4528	1.4875
4.976	1.4469	1.4938
5.038	1.4420	1.4999
5.099	1.4370	1.5060
5.160	1.4341	1.5119
5.222	1.4324	1.5177
5.283	1.4321	1.5234
5.344	1.4372	1.5289
5.406	1.4431	1.5343
5.467	1.4502	1.5396
5.528	1.4600	1.5447
5.589	1.4708	1.5497
5.651	1.4838	1.5546
5.712	1.4970	1.5594
5.773	1.5106	1.5641
5.835	1.5226	1.5686
5.896	1.5335	1.5730
5.957	1.5445	1.5773
6.018	1.5543	1.5814
6.080	1.5642	1.5854
6.141	1.5729	1.5894
6.202	1.5833	1.5932
6.263	1.5913	1.5968
6.325	1.5987	
6.386	1.6060	
6.447	1.6125	
6.508	1.6191	
6.569	1.6257	
6.631	1.6304	
6.692	1.6377	
6.753	1.6442	
6.814	1.6515	
6.875	1.6588	
6.937	1.6651	
6.998	1.6732	
7.059	1.6802	
7.120	1.6880	
7.181	1.6948	
7.242	1.7008	
7.304	1.7070	
7.365	1.7114	
7.426	1.7150	
7.487	1.7202	
7.548	1.7231	
7.609	1.7258	
7.670	1.7291	
7.731	1.7325	
7.793	1.7362	
7.854	1.7410	
7.915	1.7451	
7.976	1.7495	
8.037	1.7512	
8.098	1.7530	
8.159	1.7520	
8.220	1.7503	
8.281	1.7472	
8.342	1.7406	
8.403	1.7300	
8.464	1.7183	
8.525	1.7051	
8.586	1.6919	
8.647	1.6782	
8.708	1.6630	
8.769	1.6487	
8.830	1.6353	
8.891	1.6225	
8.952	1.6103	
9.013	1.6001	
9.074	1.5905	
9.135	1.5839	
9.196	1.5793	
9.257	1.5742	
9.318	1.5698	
9.379	1.5670	
9.440	1.5651	
9.501	1.5636	
9.562	1.5630	
9.623	1.5646	
9.684	1.5671	
9.745	1.5705	
9.805	1.5747	
9.866	1.5802	
9.927	1.5879	
9.988	1.5954	
10.049	1.6047	
10.110	1.6146	
10.170	1.6246	
10.231	1.6363	
10.292	1.6480	
10.353	1.6600	
10.414	1.6722	
10.475	1.6835	
10.535	1.6936	
10.596	1.7043	
10.657	1.7129	
10.718	1.7219	
10.778	1.7303	
10.839	1.7370	
10.900	1.7427	
10.961	1.7468	
11.021	1.7503	
11.082	1.7538	
11.143	1.7566	
11.203	1.7574	
11.264	1.7576	
11.325	1.7554	
11.386	1.7529	
11.446	1.7499	
11.507	1.7445	
11.567	1.7399	
11.628	1.7339	
11.689	1.7268	
11.749	1.7198	
11.810	1.7121	
11.871	1.7045	
11.931	1.6973	
11.992	1.6908	
12.052	1.6854	
12.113	1.6811	
12.173	1.6769	
12.234	1.6754	

Appendix B

The success of the Jacob, Thompson, and Bartell force field in the conformational analysis of hydrocarbons has already been demonstrated.[1] Certainly a workable silane force field would extend molecular mechanics into new areas. Allinger derived a force field for small silane molecules.[2] With his preliminary efforts, an attempt was made to expand his force field to accommodate larger molecules like $[(CH_3)_3Si]_3SiH$.

Allinger Force Field

Allinger's method is based on the minimization of a potential energy function in which deviations from strainless or reference point parameters increase the molecular energy. The deviations of a bond length from its "natural" value increase the molecular energy according to Hooke's law. Bond angle deformations increase the energy as the square of the angular displacement. Torsional parameters are not varied in the Allinger method but held constant while the other parameters are minimized. Finally, the nonbonded interactions are calculated by Van der Waal's functions in the manner of Hill.[4]

Allinger excludes 1,3 nonbonded interactions and bond pair interactions from the nonbonded functions because he

assumes the bonded and 1,3 effects are included at least approximately in the bond length energy term and the angular term, respectively. Hill began with an exponential-six energy expression for spherical, nonpolar molecules and obtained the following equation:

$$U = -2.25\varepsilon(r^*/r)^6 + 8.28 \times 10^5 \, \varepsilon\exp(-r/0.0736r^*) \quad (1)$$

where r^* in A° is the Van der Waal's diameter and ε in ergs is a constant for a given r^* so that the energy minimum occurs at $-1.210\ \varepsilon$. Hill listed ε and r^* for several atoms, obtaining the values from T_c, P_c, and Boltzman's constant. Allinger adopted Hill's equation but used one-half the values of r^* which Hill tabulated.

The Hill equation may be expressed in the generalized form of:

$$U = \sum_i A_i R^{B_i} \exp(-C_i R) \quad (2)$$

Where R is a length parameter and A_i, B_i, and C_i are appropriate constants. Writing the force field in terms of Equation 2 makes it compatible with the Jacob, Thompson, and Bartell (JTB) computer program.

The silane force field was derived with the H, C, and Si parameters listed at the top of Table 1. The r^* and ε for silicon are those of Ouellette[5] because Allinger's r^* appeared to be too small at 1.78 A° but his ε too large at 0.44 kcal/mole. The bottom portion of Table 1 has a tabu-

Table 1

Silane Force Field

	r*(Å)	ε(kcal/mole)	$\varepsilon(\frac{\text{mdyne A°}}{\text{molecule}})$
H[a]	1.50	0.060	4.17×10^{-4}
C[a]	1.50	0.116	8.06×10^{-4}
Si[b]	2.15	0.310	2.15×10^{-3}

$U = \sum_i A_i R^{B_i} EXP(-C_i R)$ in Millidyne A°/Molecule

Ux···y	A	B	C	A	B	C
Si···Si	-4.78×10^{-1}	-6.0	0.0	1.78×10^{3}	0.0	6.32
C···C	-2.07×10^{-2}	-6.0	0.0	6.67×10^{2}	0.0	9.09
H···H	-1.07×10^{-2}	-6.0	0.0	3.45×10^{2}	0.0	9.09
Si···C	-1.08×10^{-1}	-6.0	0.0	1.09×10^{3}	0.0	7.47
Si···H	-7.74×10^{-2}	-6.0	0.0	7.84×10^{2}	0.0	7.47
C···H	-1.49×10^{-2}	-6.0	0.0	4.80×10^{2}	0.0	9.06

[a] Allinger values.

[b] Ouellette values.

lation of the force field parameters. The energy function for like atoms is calculated directly from the Van der Waal's expression. Functions for interactions between unlike atoms are obtained by a geometric average of the respective ε's.

The bond and the angle terms in the potential energy function require force constants and reference point parameters. The spectroscopic force constants and reference parameters are given in Table 2 along with their sources.

Discussion

The geometric parameters calculated for $H_3C\text{-}SiH_3$, $(CH_3)_3SiH$, and $[(CH_3)_3Si]_3SiH$ are presented in Table 3. Only the parameters presented in Table 3 were varied. Methyl silane and trimethyl silane show no change in the geometric parameters from the reference values except for the H-Si-C-H torsion in $(CH_3)_3SiH$ where a 0.7° shift from a staggered conformation was calculated.

In $[(CH_3)_3Si]_3SiH$ the Si-Si bonded distance was left unchanged while the Si-C length decreased, but the Si-H and C-H bond lengths increased. The angle changes are more pronounced especially the Si-Si-H angle which dropped 0.6° from the 109.0° reference. The decrease suggests that the molecule relieves the steric strain of the bulky trimethylsilyl groups through the Si-Si-H angle as it moves to a value smaller than the tetrahedral angle.

Table 2

Conformational Analysis Parameters[a]

Parameter	Force Constant[b]	Reference Point[c]
Si-H Bond	2.72	1.484
Si-Si Bond	1.73[d]	2.361[e]
Si-C Bond	2.92	1.872
C-H Bond	4.6	1.094
Si-Si-H Angle	0.48	109.°
C-Si-Si Angle	0.48	110.5°
Si-C-H Angle	0.476[f]	110.0°
C-Si-Si-H(1) τ	0.5[f]	60°
H-C-Si-Si τ	0.5[f]	60°

[a] Parameters not marked are those of Allinger.

[b] Bonds in millidyne A°, angles in millidyne A°/rad^2 torsions as rotational barriers in kcal/mole for use in the JTB computer program.[1]

[c] Bonds in A°, angles in degrees.

[d] J. L. Duncan, Spectrochim. Acta, 20, 1807 (1964).

[e] L. S. Bartell, F. B. Clippard, Jr., and T. L. Boates, Inorg. Chem., 9, 2436 (1970).

[f] R. J. Ouellette, D. Beron, J. Stolfo, A. Rosenblum, and P. Weber, Tetrahedron, 28, 2163 (1972).

Table 3

Results (Best Values)

Parameter[a]	H_3CSiH_3	$(CH_3)_3SiH$	$[(CH_3)_3Si]_3SiH$
Si-H Bond	1.484	1.484	1.485
Si-Si Bond	----	----	2.361
Si-C Bond	1.871	1.871	1.870
C-H Bond	1.094	1.094	1.095
Si-Si-H Angle	----	----	108.4
C-Si-Si Angle	----	----	110.5
Si-C-H Angle	110.0	110.0	109.9
C-Si-Si-H τ	----	----	50.0
H-C-Si-Si τ	----	----	-0.16
H-Si-C	110.5	110.5	----
H-Si-C-H	60	60.7	----

[a] Bonds in A°, angles in degrees.

The C-Si-Si-H torsion at 50° or 10° from the reference staggered configuration is the greatest deviation from the strainless value. The initial value of 45° was increased as the parameter moved in the direction of the experimental value. Otherwise, the deviations from the reference parameters are small and not in keeping with the experimental values presented earlier. In the cases of $(SiH_3)_2CH_2$ and $H_2C = CHSiH_3$, the results published by Allinger[2] show serious discrepancies between observed geometries and the calculated values.

Appendix C

A gas phase electron diffraction study of tris(trimethylsilyl) methane was begun but not completed because the compound decomposed during the experiment. The investigation was undertaken to compare the geometric parameters with those determined for tris(trimethylsilyl) silane. A sample of $[(CH_3)_3Si]_3CH$ sealed in a glass vial was received from Dr. H. Bürger. The same experimental procedures were employed for obtaining the diffraction patterns as were outlined in Part I. Two sample containers of the same design were fitted into a Y-shaped connector which was joined to the nozzle as previously described. For a given camera distance, photographic plates were exposed alternately with the two compounds. Experimental conditions are presented in Table 1.

Analysis of Data

The diffraction patterns recorded on 4 x 5 inch photographic plates were processed in the same manner as in Part I. Diffraction intensities, after conversion to plate exposures, were measured on a digital recording microphotometer. The molecular description appears in Table 2.

During the data analysis, serious contamination of the sample was detected by the large oscillations in the correlation background. The correlation background function[1]

APPENDIX C

Table 1

Experimental Conditions for $[(CH_3)_3Si]_3CH$

	I	II	III
Camera Distance	21.401	10.706	21.233
Sector (radius, mm)	$R^3(44)$	$R^3(44)$	$R^2(25)$
Nozzle Temperature (°C)	101	130	120
Sample Pressure (torr)	10	28	25
Exposure Time (sec)	3	12	0.5
Beam Current (μA)	0.70	0.70	0.70
Platinum Nozzle diam., mm	0.3	0.3	0.3
Number of plates averaged	2	5	5

Table 2

Molecular Description for $[(CH_3)_3Si]_3CH$

Geometric Parameters

Para No.		
1	C-H (1)	Bond
2	Si-C	Bond
3	C-H	Bond
4	Si-C-H (1)	Angle
5	C-Si-Si	Angle
6	$Si-C-H_{methyl}$	Angle
7	C-Si-C-H (1)	Torsional angle
8	H-C-Si-C	Torsional angle
9	Silicon tilt	Angle

Amplitudes of Vibration

1	Si···Si (1,3)
2	Si-C (1,2)
3	Si···C (1,4)G[a]
4	Si···C (1,4)T[b]
5	Si···H (1,3)
6	Si···H[c]
7	C···C (1,3)
8	C···C (1,5)GG
9	C···C (1,5)GT
10	C···C (1,5)TT
11	C-H (1,2)
12	C···H (1,6)
13	C···H (1,4)
14	H···H (1,3)
15	H···H Long 1
16	H···H Long 2
17	H···H Long 3

---

[a] gauche.

[b] trans.

[c] All Si···H amplitudes other than the (1,3) amplitude.

should be quite smooth. Consequently structural parameters were not determined for the molecule.

Results and Discussion

After the experiments were completed, it was learned that tris(trimethylsilyl)methane decomposes with age.[2] The sample container had been stored in a conventional refrigerator prior to taking the diffraction patterns. A colorless liquid was transferred into the sample tank whereas the decomposition products were described as forming a white solid.

Quite possibly the compound decomposed when it was heated to increase its vapor pressure. Possible mechanisms of reaction are the displacement of the trimethylsilyl groups via a carbonium ion or free radical attack by the tertiary carbon, leading to a number of silyl by-products. An alternative reaction would be the tertiary hydrogen elimination and recombination at the tertiary carbons to form $[(CH_3)_3Si]_3C\text{-}C[Si(CH_3)_3]_3$.

APPENDIX D: COMPUTER PROGRAMS

Computer card decks, punched during the intensity measurements on the microphotometer, for each photographic plate, are formatted to run through VCCD which checks for centering and voltage drift. The right and left sides of the plates are averaged in VCCD and are ready for leveling. Experimental levelled intensities are calculated by ELI which takes into account the experimental conditions for each of several plates, the corrections for flat plates and the photographic emulsion constants and averages the intensities of the several plates for a given camera distance. The ELI program produces a deck of cards with intensities at non-integral q values. Before running ELI, atomic intensities must be calculated by TABSCATR which employs the tabulated elastic[1] and inelastic[2] scattering factors and the phase shifts.[1]

Intensities at integral q are calculated by INTERP. After interpolation the data sets are ready for background calculations by LSI, the least squares of the intensities program. There is also AHKLSI available which is the LSI program expanded to 200 internuclear distances instead of only 150. Both AHKRED and AHKSUB (the redimensioned READQ and subroutine package, respectively) must be specified on the $RUN card with AHKLSI. The program LSI is complete. Weighting subroutines, designated by WT, are capable of weighting the intensities as desired by the

program operator.

Fourier sine transforms of the reduced molecular intensities can be calculated and plotted by FR for a visual check of the structural analysis. After suitable background functions for each camera distance have been obtained with LSI or AHKLSI, the data of the individual camera distances are combined by BLEND into a composite molecular intensity. Often a check on the initial structure is beneficial. So internuclear distances can be calculated for a trial structure by MODIST which converts internal coordinates to Cartesian coordinates with the LINUS subroutine. Force field calculations in this thesis were made with DIPSY VI although other versions are also available.

The above programs represent the basic routines needed for an electron diffraction structural analysis. Detailed accounts of these programs are on file with the electron diffraction group at The University of Michigan. Programs which are limited in scope and not generally used in the structural analysis have not been described in this dissertation. The reader is referred to the program book for details on these programs.

The three-atom calculations are made by CORINT which is stored as CLRCORK2. The least squares refinement is made with CLRLSI2 which calculates the three-atom corrections and adds them to the theoretical reduced molecular intensity. Perpendicular amplitudes of vibration for

CLRLSI2 are calculated by ZAMP3. The standard WT subroutines are used with CLRLSI2. A theoretical background and the scattering factor derivatives for CLRLSI2 must first be calculated with CLRTABLE. The corrections alone may be calculated with CLRINT or AKINT which lists the real and imaginary portions of E(S).[3]

References, Appendix B.

1. E. Jean Jacob, H. Bradford Thompson, and L. S. Bartell, J. Chem. Phys., 47, 3736 (1967).

2. M. T. Tribble and N. L. Allinger, Tetrahedron, 28, 2147 (1972).

3. T. L. Hill, J. Chem. Phys., 16, 399 (1948).

4. R. J. Ouellette, D. Baron, J. Stolfo, A. Rosenblum, and P. Weber, Tetrahedron, 28, 2163 (1972).

References, Appendix C.

1. L. S. Bartell in Physical Methods in Chemistry, A. Weissberger and B. N. Rossiter, Eds., 4th Edition, Interscience Publishers, New York, 1973.

2. H. Bürger (private Communication).

References, Appendix D.

1. L. Schafer, A. C. Yates, and R. A. Bonham, J. Chem. Phys., 55, 3055 (1971).

2. C. Tavard, D. Nicolas, M. Rouault, J. Chim. Phys., 64, 540, 555 (1967).

3. T. C. Wong and L. S. Bartell, J. Chem. Phys., 58, 5654 (1973).